7586–7611 *Nucleic Acids Research, 2018, Vol. 46, No. 15* *Published online 16 July 2018*
doi: 10.1093/nar/gky618

Integrating Rio1 activities discloses its nutrient-activated network in *Saccharomyces cerevisiae*

Maria G. Iacovella[1], Michael Bremang[1,2,†], Omer Basha[3,†], Luciano Giacò[1,†], Walter Carotenuto[4], Cristina Golfieri[1], Barnabas Szakal[4], Marianna Dal Maschio[1], Valentina Infantino[1], Galina V. Beznoussenko[4], Chinnu R. Joseph[4], Clara Visintin[1], Alexander A. Mironov[4], Rosella Visintin[1], Dana Branzei[4,5], Sébastien Ferreira-Cerca[6], Esti Yeger-Lotem[3] and Peter De Wulf[1,7,*,‡]

[1]Department of Experimental Oncology, European Institute of Oncology, Via Adamello 16, 20139 Milan, Italy, [2]Current address: Proteome Sciences Plc, Hamilton House, Mabledon Place, London, United Kingdom, [3]Department of Clinical Biochemistry and Pharmacology, Faculty of Health Sciences and the National Institute for Biotechnology in the Negev, Ben-Gurion University of the Negev, POB 653, Beer-Sheva 84105, Israel, [4]The FIRC Institute of Molecular Oncology (IFOM), Via Adamello 16, 20139 Milan, Italy, [5]Istituto di Genetica Molecolare, Consiglio Nazionale delle Ricerche (CNR), Via Abbiategrasso 207, 27100 Pavia, Italy, [6]Lehrstuhl für Biochemie III, Universität Regensburg, Universitätsstraße 31, 93053 Regensburg, Germany and [7]Centre for Integrative Biology (CIBIO), University of Trento, Via Sommarive 9, 38123 Trento, Italy

Received January 10, 2018; Revised May 29, 2018; Editorial Decision June 26, 2018; Accepted June 28, 2018

ABSTRACT

The *Saccharomyces cerevisiae* kinase/adenosine triphosphatase Rio1 regulates rDNA transcription and segregation, pre-rRNA processing and small ribosomal subunit maturation. Other roles are unknown. When overexpressed, human ortholog RIOK1 drives tumor growth and metastasis. Likewise, RIOK1 promotes 40S ribosomal subunit biogenesis and has not been characterized globally. We show that Rio1 manages directly and via a series of regulators, an essential signaling network at the protein, chromatin and RNA levels. Rio1 orchestrates growth and division depending on resource availability, in parallel to the nutrient-activated Tor1 kinase. To define the Rio1 network, we identified its physical interactors, profiled its target genes/transcripts, mapped its chromatin-binding sites and integrated our data with yeast's protein–protein and protein–DNA interaction catalogs using network computation. We experimentally confirmed network components and localized Rio1 also to mitochondria and vacuoles. Via its network, Rio1 commands protein synthesis (ribosomal gene expression, assembly and activity) and turnover (26S proteasome expression), and impinges on metabolic, energy-production and cell-cycle programs. We find that Rio1 activity is conserved to humans and propose that pathological RIOK1 may fuel promiscuous transcription, ribosome production, chromosomal instability, unrestrained metabolism and proliferation; established contributors to cancer. Our study will advance the understanding of numerous processes, here revealed to depend on Rio1 activity.

INTRODUCTION

The RIO family of atypical protein kinases is found in most archaea, bacteria and eukaryotes (1–5). Lower eukaryotes including the budding yeast *Saccharomyces cerevisiae* comprise two subfamilies: Rio1/RIOK1 and Rio2/RIOK2, while higher eukaryotes, including humans, contain an additional subfamily: RIOK3. From archaea to higher eukaryotes, Rio1 promotes the 3′-end processing of the small ribosomal subunit pre-rRNA and mediates the release of late biogenesis factors during small ribosomal particle maturation. Importantly, as far as the process of ribosome biogenesis is concerned, Rio1 can act as a kinase as well as an adenosine triphosphatase (ATPase) (6–15). In budding

*To whom correspondence should be addressed. Tel: +39 0461285359; Fax: +39 0461283937; Email: peter.dewulf@unitn.it
†The authors wish it to be known that, in their opinion, the third and fourth authors should be regarded as Joint Second Authors.
‡Lead contact.

yeast, Rio1 kinase activity also regulates *35S* rDNA transcription by RNA polymerase I to ensure a timely onset of the cell cycle, to safeguard rDNA copy-number homeostasis, and to promote rDNA condensation and segregation (16). Its involvement in rDNA and rRNA biology, and its promotion of 40S ribosomal subunit maturation are consistent with *RIO1* being a member of the ribosome biogenesis (Ribi) regulon (17–19). The latter comprises 236 genes whose proteins participate in the synthesis, assembly and functioning of the ribosome. Importantly, they do not encode the structural components of the ribosome as these are encoded by the ribosomal protein (RP) regulon. Ribi and RP expression are co-regulated in response to environmental conditions and the ability of a cell to grow and proliferate therein (e.g. nutrient availability): activated when resources are abundant, repressed when they are scarce (17–19). Heterozygous *rio1Δ* yeast is sensitive to drugs perturbing Golgi activity, DNA replication, sphingolipid and ergosterol biosynthesis (20). These phenotypes suggest an involvement of Rio1 also in these processes, beyond ribosome biology.

In human cells, next to its role as a ribosome biogenesis factor (21–23), RIOK1 has also been implicated in the regulation of intracellular signaling, gene expression, cancer initiation, development and metastasis. Indeed; RIOK1 phosphorylates the TORC2 kinase complex to activate the kinase AKT and its downstream signaling network (24). RIOK1 is also part of the PRMT5 arginine N-methyltransferase complex, which methylates, among others, histone H4R3 to silence globin expression (25) and the ribonucleoprotein hnRNP A1 to control the translation of the cyclin D1 and c-Myc transcripts (26). A genetic lethality screen in colon cancer cells expressing the oncogenic $KRAS^{G13D}$ mutation identified *RIOK1* (27), suggesting involvement of RIOK1 in the activity of the GTPase KRAS. The latter functions as a molecular switch for signaling pathways that regulate growth, survival, proliferation, differentiation, migration and cytoskeletal dynamics (28,29). Knocking down RIOK1 in KRAS-addicted cancers impaired their ability to proliferate and invade (30), pointing to treatment options, for example via RIOK1 inhibitors (31–33).

Although *RIOK1* overexpression promotes cancer growth and invasion (30) its contributions to both events remain unclear because the protein -as is true also for Rio1- has not yet been mapped functionally at the whole-cell level. To advance our understanding of Rio1 and RIOK1 biology, we charted Rio1 activity in *S. cerevisiae*. Next, we revealed its functional conservation from yeast to human cells. Specifically, we identified physical and functional interactors of Rio1 by yeast two-hybrid and genetic synthetic screens, the genes and/or transcripts it regulates by RNA-sequencing, we localized Rio1 across the genome via ChIP-sequencing analysis and throughout the cell by indirect immunofluorescence (IF) and cryo-immunogold electron microscopy (EM). Using network computation we integrated our biological datasets with empirically verified and curated yeast protein–protein and protein–DNA interaction catalogs. This effort produced Rio1's multi-layered network, which functions at the protein, gene/chromatin and RNA levels. Rio1 controls its target open reading frames (ORFs) both directly and indirectly using a host of transcription factors and regulators. Combined, the identities of its gene targets, protein interactors and intracellular localization patterns suggest that Rio1 regulates ribosome production, protein synthesis and turnover, metabolism, energy production and cell division (rDNA replication and chromosome transmission). *RIO1* transcription, which we find is auto-regulated, is high under nutritionally rich conditions. Upon nutritional deprivation (glucose, amino acids), *RIO1* expression becomes auto-repressed and the translation of its few transcripts increases. This pattern of regulation correlates with the expression status of its network regulon members, as indicated by a host of reporter genes involved in the most divergent intracellular processes. Noteworthy, Rio1 and nitrogen stress-response transcription factor Gcn4 cross-regulate each other and their gene networks in adaptation to growth conditions. Our singular datasets and tractable activity map represent valuable resources revealing how Rio1 and its network manage various essential biological processes, now associated with Rio1 activity.

MATERIALS AND METHODS

Yeast strains and culture conditions

The *S. cerevisiae* strains used in this study (Supplementary Table S14) have a W303-1A genetic background and were created by mating, tetrad dissection followed by spore selection, or by transformation and homologous recombination of polymerase chain reaction (PCR)-generated deletion or epitope cassettes. The *RIO1-AID, P_{ADH1}-OsTIR1-9Myc* degron strain (next named the *RIO1-AID* strain) was engineered as described (34). Strains were grown exponentially (OD_{600} = 0.8–1.0) at 24°C (200 rpm) in YPD (1% yeast extract, 2% peptone, 2% glucose) or YPRG medium (1% yeast extract, 2% peptone, 2% raffinose, 2% galactose). To deplete Rio1 from yeast, exponentially growing *RIO1-AID* cells were treated for 1 h with 500 μM of auxin (indole-3-acetic acid; Sigma-Aldrich, Cat # I3750). Rio1-AID depletion was confirmed by anti-AID western blot hybridization and by RT-qPCR analysis of *35S* pre-rRNA transcript levels. For the starvation experiments; *RIO1-AID* cells were grown in synthetic complete medium (0.67% yeast nitrogen base without amino acids (Difco, Cat # 291940), 2% glucose, 0.002% amino acid drop-out mix), collected, washed with water, and re-suspended in synthetic drop-out medium (0.67% yeast nitrogen base without amino acids) provided with 2% glucose or with 0.002% amino acid drop-out mix, and supplemented with 500 μM of auxin or mock solution. One hour after being shifted to the new growth medium, the cells were collected, all RNAs extracted, and converted into cDNA for quantitation of certain cDNAs using a set of TaqMan RT-qPCR probes.

Yeast two-hybrid interaction screens, and confirmation by co-immunoprecipitation and western blot hybridization analysis

Yeast two-hybrid (Y2H) screens were performed by Hybrigenics Services (www.hybrigenics-services.com; Paris, France). The *RIO1* coding sequence (YOR119C) was fused in frame at its N- or C-terminus to the LexA or the Gal4

DNA-binding domain. The four bait constructs were then screened three times each against all *S. cerevisiae* genes, fused N- or C-terminally to the Gal4 activation domain. In the screens, the complexity of the *S. cerevisiae* genomic library was covered 5- to 14-fold. Prey fragments of positive clones were amplified by PCR, sequenced and identified in the GenBank database (NCBI). Next, a predicted biological score (*e*-value) was calculated for each identified interaction. First, a local score took into account the redundancy and independency of the prey fragments, as well as the distribution of reading frames and stop codons in overlapping fragments. Second, a global score considered the interactions found in all the screens performed previously with the same genomic library. The combined calculated score (*e*-value $\leq$ 1.0E-02) positively correlates with the biological significance of the identified interaction (35–38).

To corroborate biochemically that Rio1 physically interacts with Y2H hits Rvb2, Sky1 and Sam37, we performed co-immunoprecipitation (co-IP) experiments. Since the endogenous expression level of *RIO1* is very low, and given that the efficacy of co-IP and elution of the interacting proteins is very low as well, we decided to perform the co-IP analysis using strains in which the expression of *RIO1*, *RVB2*, *SKY1* and *SAM37* were slightly elevated (details below) allowing for the identification of the Rio1-protein interaction by western blot hybridization analysis. Specifically, we created four strains in which the *RIO1* coding sequence was N-terminally labeled with a tandem 1FLAG-PrA (protein A) tag. Next, in three strains, the *RVB2*, *SKY1* or *SAM37* coding sequence was marked with an N-terminal 3HA epitope (in the fourth, negative control strain, no protein was labeled with a 3HA epitope). The expression of the proteins was placed under control of the P_{GAL1} promoter and the strains then grown in 2% raffinose YP medium (YPR) to slightly enhance protein levels. Cell extracts were made with acid washed glass beads (FastPrep FP120 homogenizer, MP Biomedicals) and incubated for 4h (at 4°C) with anti-1FLAG M2 affinity agarose beads (Sigma, Cat # A2220). The beads were washed three times with phosphate-buffer saline (PBS) (pH 7.4) supplemented with 1% Triton X-100. Next, the beads were incubated with 1FLAG peptide (Sigma, Cat # F3290) at different concentrations (up to 250 μg/ml; overnight, 4°C). Since the added peptide proved to poorly detached 1FLAG-PrA-Rio1 from the affinity beads, the latter were rewashed five more times, resuspended in sodium dodecyl sulphate (SDS) loading buffer and briefly boiled for 60 s. Following centrifugation, bead-free supernatant was submitted to sodium dodecyl sulphate-polyacrylamide gel electrophoresis (SDS-PAGE) (4–20% Mini-Protean TGX precast gel; BioRad Cat # 4561093) and both anti-FLAG (mouse monoclonal anti-FLAG M2 (1:4000; Sigma-Aldrich Cat # A2220) and anti-HA (mouse monoclonal anti-HA 16B12 (1:1000; Covance Cat # MMS-101P)) western blot hybridization analysis (lanes labeled with 'IP'). Cell extracts not submitted to the IP procedure were analyzed using the same anti-FLAG and anti-HA western hybridization protocols (lanes labeled with 'Input'). Specifically, the IP and input fractions were split in two; one half of the input and one half of the IP were run out in parallel on one gel, the other halves were run out on a second gel. After transferring the proteins onto Immobilon-P PVDF membranes (Millipore, Cat # IPVH00010), one membrane was hybridized with primary anti-FLAG antibody, the other with a primary anti-HA antibody (see above). Of note; the IPs submitted to anti-HA western blot analysis also detected traces of the IgG heavy chain of the agarose-bound mouse anti-FLAG antibody due to hybridization with the mouse horseradish peroxidase-conjugated secondary antibody (goat anti-mouse (1:10 000; BioRad Cat # 170–6516)). The PrA epitope also hybridizes with the IgG heavy chain of primary and secondary antibodies, as indicated in Supplementary Figure S1B.

Western blot hybridization analysis of Rio1-AID protein levels

Cells were collected from a 5 ml culture sample (14 000 rpm; 1 min, 4°C), treated with 5% trichloroacetic acid (Sigma-Aldrich) and processed as described (16). Membranes (Immobilon-P PVDF; Millipore) were incubated with mouse monoclonal anti-AID antibody (1:1000; Cosmo Bio Co., Cat # BRS-APC004AM) or with mouse monoclonal anti-Pgk1 antibody (1:5000; Life Technologies, Cat # 459250). Following incubation with horseradish peroxidase-conjugated goat anti-mouse secondary antibody (1:10 000; BioRad, Cat # 170–6516) the proteins were visualized using ECL chemiluminescence solution (GE Healthcare) and radiography (GE Healthcare).

Serial dilution growth analysis

Yeast strains were grown overnight at 24°C (200 rpm) in YPD or YPR medium, back-diluted to an OD_{600} = 1.0, and serially diluted (1:4.5 dilution steps) in 96-well plates. The cells were transferred with a multi-pin replicator from the multi-well plates onto YPD or YPRG agar plates and incubated for 2–3 days at the indicated temperatures (Supplementary Figures S2B-C and 3A).

Indirect immunofluorescence widefield imaging and cryo-immunogold electron microscopy

Indirect IF widefield deconvolution imaging of yeast cells endogenously expressing 6Myc-Rio1, Rio1-GFP, Ndc80-3GFP or Nop1, or of nuclei isolated from the cells, was performed as described (16). In short, a 1 ml sample of yeast cells grown exponentially in YPD medium (24°C, 200 rpm) was centrifuged and cross-linked overnight in 1 ml of 3.7% formaldehyde. The cell walls were then digested (30 min) with zymolyase (100 μg ml^{-1}, Amsbio Cat # 100T), washed with 1.2 M sorbitol plus 100 mM phospho-citrate pH 5.9, and bound to a multiwall poly-L-lysine coated glass slide (Sigma-Aldrich). The slide was treated with DAPI, and hybridized with a rabbit anti-GFP primary antibody (Living Colours Full-Length GFP Polyclonal Antibody, Clontech, Cat # 632593), a mouse monoclonal anti-Myc primary antibody (9E10, Covance, Cat # MMS-150R) or a mouse monoclonal anti-Nop1 primary antibody (ThermoFisher, Cat # 28F2). CY3 or fluorescein isothiocyanate (FITC)-labeled secondary antibodies (Jackson ImmunoResearch Laboratories) were used to visualize the proteins. Images were cap-

tured with a DeltaVision ELITE microscope (Applied Precision) carrying an Olympus IX71 UPlanSApo objective lens (100×, NA 1.40) and a CoolSnap HQ2 CCD camera (Photometrics). Fifteen Z-stacks were acquired every 0.4 μm, deconvoluted (SoftWoRx) and vertically projected with maximum intensity.

Cryo-immunogold EM was performed as described (39). In short, *S. cerevisiae* cells endogenously expressing Rio1-GFP were grown in YPD medium (200 rpm, 24°C) till an $OD_{600} = 0.8$. Next, the cells were pelleted by centrifugation, embedded in 12% gelatin, cooled on ice and cut into 1 mm^3 cubes at 4 °C. The cubes were immersed in 2.3 M sucrose (4 °C, overnight), fast-frozen in liquid nitrogen, and cut with a Leica EM FC7 ultramicrotome. Thin sections (50–60 nm thickness) were picked up in a 1:1 mix of 2% methylcellulose and 2.3 M sucrose, and incubated with the rabbit anti-GFP antibody (1:10 dilution). Next, the sections were incubated with gold (10 nm)-labeled protein A (Cell Microscopy Center, University of Utrecht Medical School, The Netherlands), treated with 1% glutaraldehyde and embedded in methylcellulose uranyl acetate. Images were acquired with a Tecnai-20 electron microscope (FEI, Eindhoven, The Netherlands). To calculate the volumes of cells and organelles, we used the discretized version of the vertical rotator procedure. Specifically, we drew the central vertical axis through the center of the maximal diameter of the cell and then placed the stereological grids, as published (40). The gold labeling density was quantitated as described (41). For the nucleus, mitochondria and vacuoles, the numeric volume density (gold/μm^2) was quantitated, whereas for the plasma and Golgi membranes, we measured the numeric surface density (gold/μm).

Fluorescence-activated cell sorter (FACS) analysis

Per time point, 1×10^7 cells were collected by centrifugation and resuspended in 70% ethanol for 16 h. The cells were then washed in 250 mM Tris–HCl (pH 7.5), resuspended in this buffer containing 2 mg/ml of RNase A (37°C, 4 h) and treated with proteinase K (1 mg/ml) (37°C, 30 min). Next, the cells were resuspended in 200 mM Tris–HCl (pH 7.5), 200 mM NaCl and 80 mM $MgCl_2$ and their DNA then stained with 1 μM Sytox-green (Invitrogen). Samples were diluted 10-fold in 50 mM Tris–HCl (pH 7.8) and analyzed with a Becton Dickinson FACScan instrument.

Extraction of replication intermediates and analysis by 2D agarose gel electrophoresis

Purification of DNA intermediates and 2D agarose gel electrophoretic analysis were performed as described (42). In short, following the synchronous release of cells enriched in late G1 (START) using α-factor, a 200 ml culture of *RIO1-AID* cells containing or depleted of Rio1-AID and arrested with 200 mM of hydroxyurea (HU), were sampled ($2–4 \times 10^9$ cells), treated with 0.1% NaN_3, spheroplasted and submitted to DNA extraction with chloroform:isoamylalcohol (24:1). Next, the purified DNA was treated with restriction enzymes EcoRV and HindIII to analyze ARS305, or with BglII to analyze *5S* rDNA, separated using 2D agarose gel electrophoresis, and submitted to Southern blot hybridization with radiolabeled probes targeting ARS305 and *5S* rDNA (43). Recombination intermediate signals were quantitated with ImageQuant software (GE Healthcare). For each time point, areas corresponding to the monomer spot (M), the Y arc and a region without replication intermediates (background reference) were selected and the signal intensities in % of each signal obtained. The values for the Y arc and monomer were corrected by subtracting from the signal intensity value the background value after the latter was multiplied for the ratio between the dimension of the area for the intermediate of interest and for the background. The relative signal intensity for the Y arc was determined by dividing the value for Y arc/termination with the monomer values.

RNA isolation

Total RNA was isolated from 5 ml of an exponential culture. The cells were harvested (14 000 rpm, 1 min, 4°C), washed with ice-cold buffer (50 mM sodium acetate pH 5.2, 10 mM ethylenediaminetetraacetic acid (EDTA) pH 8.0) and stored at −80°C. RNA was then extracted using phenol and chloroform, as described (16). Next, residual DNA was removed by incubation (30 min, 37°C) with DNase I (New England Biolabs, Cat # M0303S) and the RNA further purified with the RNeasy Kit (Qiagen, Cat # 74104). RNA concentrations were measured with a NanoDrop 2000c UV-Vis Spectrophotometer (ThermoFisher Scientific) and its quality and integrity examined with a 2100 Bioanalyzer (Agilent Technologies).

Real-time qPCR (RT-qPCR)-based quantitation of RNA transcripts

A total of 1 μg of RNA, isolated as indicated above, was reverse transcribed into cDNA with ImProm-II reverse transcriptase (Promega, Cat # A3801) and random primers (Life Technologies, Cat # 48190-011). A total of 5 ng of the cDNA were then submitted to RT-qPCR analysis (7500 Fast Real-Time PCR, Life Technologies) using either custom-made or commercially available TaqMan probes (ThermoFisher Scientific). The custom-made ETS1-1 probe (named probe nr. 4) measures the cDNAs derived from the primary *35S* pre-rRNA transcripts at the *5′ETS* sequence;

- forward primer: 5′-GATTTGGTGGATTACTAGCTA ATAGCAATCT-3′,
- reverse primer: 5′-GGAGGTTACACTTGAAGAATC ACAGT-3′,
- reporter sequence: 5′-CAACAAGGCATTCCCC-3′, 5′-fluorophore: 6-carboxyfluorescein (FAM), 3′-quencher: non-fluorescent quencher (NFQ)).

The custom-made RPL7B probe measures the cDNAs derived from the *RPL7B* transcripts;

- forward primer: 5-GAAAGAAACATCATTCAAGCT AAGCGT-3′,
  reverse primer: 5′-GTTGAGCTTCGACGTAGTAGG AA-3′,
- reporter sequence: 5′-CAGCAGCCTTGGCATC-3′, 5′-fluorophore: FAM, 3′-quencher: NFQ.

The commercially available TaqMan RT-qPCR probes used in this study (ThermoFisher Scientific) are listed in Supplementary Table S15.

Ribosome profiling, pulse labeling of neo-synthesized RNAs and proteins

Ribosome profiles (40S and 60S subunits, 80S monosomes and polysomes) were produced by growing the *RIO1* wild-type and *RIO1-AID* strains to an OD_{600} = 0.5 in YPD medium (24°C). The cells were then treated for 1 h with 500 μM of auxin, isolated, treated on ice (5 min) with 100 μg ml^{-1} cycloheximide (to stabilize the polysomes), and washed with extraction buffer (20 mM Tris–HCl pH 7.5, 50 mM KCl, 10 mM $MgCl_2$, 100 μg ml^{-1} cycloheximide). The cells were broken with glass beads and the cleared extract loaded on a 10.5 ml 5–45% sucrose gradient in extraction buffer lacking cycloheximide. Following centrifugation (16 h; 21 000 rpm; SW41 Beckman rotor), gradients were collected at a 1 ml min^{-1} flow rate and the UV profile recorded at 254 nm with a UV detector (linked to BioLogic LB fractionators), visualized with LP Data View software (Bio-Rad) and exported to Excel (Microsoft Office).

To study whether a 1 h depletion of Rio1 affected (r)RNA production we grew the *RIO1* wild-type and *RIO1-AID* strains overnight in 2% glucose synthetic medium containing 10 mM uracil. The cells were then back-diluted in 2% glucose synthetic medium comprising 2.5 mM uracil, grown for two generations and treated with 500 μM auxin for 1 h. Forty min into the auxin treatment, 7.5 mM 4-thiouracil (4TU) (Sigma-Aldrich, Cat # 440736) was added to the cultures. The cells were harvested after 20 min and total RNA extracted (16). The newly synthesized, 4TU-incorporated RNAs were biotinylated in the dark using 5 μg MTSEA Biotin-XX (Biotium, Cat # 90066) (44) in 10 mM Tris–HCl pH 7.4 plus 1 mM EDTA pH 8.0 for 30 min. Biotinylated RNAs were purified by hot-phenol extraction, 5–10 μg separated by denaturing agarose gel electrophoresis, transferred onto a positively charged nylon membrane and UV-crosslinked. To detect the fluorescent 4TU-labeled RNAs, the membranes were incubated for 20 min in blocking solution (1× PBS pH 7.5, 1 mM EDTA pH 8.0) containing 10% (w/v) SDS under mild agitation. Subsequently, the membranes were incubated in the dark (24°C, 20 min) under mild agitation with IR-dye conjugated streptavidin (1:10 000 dilution in blocking solution containing 10% SDS—IRDye 800CW Streptavidin (LI-COR, Cat # 926–32230)). The membranes were then washed twice (10 min each) with blocking solution containing a decreasing concentration of SDS (10%, 1 and 0.1%). Labeled RNAs were visualized on a LI-COR Odyssey imaging platform (as described in (45)).

To quantitate the translation capacity of yeast depleted of Rio1 for 1 h, the *RIO1* and *RIO1-AID* strains were grown at 24°C in complete 2% glucose synthetic medium till an OD_{600} = 5.0, at which point 500 μM of auxin was added. After 40 min, the cells were washed with and resuspended in 1 ml of 2% glucose synthetic medium lacking methionine but containing 500 μM of auxin. A total of 100 μCi of 5′,6′ [^{3}H]-L-methionine (Hartmann Analytic) was added for 20 min at 24°C. Next, all proteins (TCA insoluble fraction) were extracted, washed twice with cold acetone and solubilized in SDS-loading buffer. The solubilized proteins were separated on a Nu-PAGE 4%-10% gel (Invitrogen). The gel was then dried and the amount of newly synthesized proteins with incorporated 5′,6′ [^{3}H]-L-methionine quantified with a scintillation counter. In parallel, the proteins were separated on a 4–10% gel and coomassie-stained to confirm equal loading.

RNA-Sequencing (RNA-Seq) and data analysis

To profile and compare all transcripts present in yeast that either contains or is depleted of Rio1, *RIO1-AID* cells were grown in YPD medium (24°C, 200 rpm, OD_{600} = 0.6–1.0) and then treated for 1 h with 500 μM of auxin or with a mock solution. A total of 5 μg of total RNA were isolated as described above, and ribosomal RNAs (rRNAs) removed with the Ribo-Zero Gold rRNA Removal Kit Yeast (Illumina, Cat # MRZY1324). rRNA depletion was confirmed by 2100 Bioanalyzer RNA6000 Pico Chip analysis (Agilent Technologies). A total of 2 μl of the rRNA-depleted RNAs were then reverse transcribed into a cDNA library with the ScriptSeq v2 RNA-Seq Library Preparation Kit (Illumina, Cat # SSV21124). cDNA library concentrations were quantified with a Qubit Fluorometer (Invitrogen) and its quality examined on a 2100 Bioanalyzer using the High Sensitivity DNA assay (Agilent Technologies). The cDNA library was then deep sequenced in multiplex fashion (6 samples per run) for 75 bases in the paired-end mode on a MiSeq Sequencing System (Illumina).

The library reads were aligned on the reference genome sacCer3 (*S. cerevisiae* S288c assembly from the *Saccharomyces* Genome Database (GCA_000146055.2)) (46) using TopHat software (47). The mapped sequences were processed with HTSeq software (48) using parameters: (-m) intersection strict, (-a) skip quality reads less than 1. Differential gene expression analyses including size-factor normalization, shrinkage estimation for the distribution's variance and negative binomial distributions were performed using the R package DESeq (49).

Chromatin immunoprecipitation (ChIP), ChIP∼RT-qPCR and ChIP-chip analysis

RIO1-AID cells were grown exponentially till an OD_{600} = 0.8 in YPD medium (24°C, 200 rpm). Culture samples (50 ml) were then cross-linked with 1% formaldehyde (24°C, 1 h) and treated as described (16). Mouse monoclonal anti-AID antibody (10 μl) (Cosmo Bio Co., Cat # BRS-APC004AM) conjugated to protein A-agarose beads (ThermoFisher Scientific, Cat # 15918014) was then used to isolate Rio1-AID from the cell extracts. After washing and resuspending the beads, the crosslinks were reversed overnight (1% SDS, 65°C). All proteins were removed with Proteinase K (Roche, Cat # 03115828001) and contaminant RNA degraded with RNase A (Sigma-Aldrich, Cat # 10109169001). The chromatin that co-immunoprecipitated with Rio1-AID was extracted with phenol and chloroform, resuspended in 40 μl of double-distilled water and quantified with a NanoDrop 2000c UV-Vis Spectrophotometer (ThermoFisher Scientific). In a first set of parallel negative

control ChIP experiments; *RIO1-AID* cells were submitted to the ChIP protocol in which only protein A beads were used (no anti-AID antibody). In a second set, the untagged *RIO1* wild-type yeast was subjected to the ChIP protocol in the presence or absence of anti-AID antibody (protein A beads used).

The amount of rDNA chromatin that co-immunoprecipitated with Rio1-AID was quantitated by TaqMan RT-qPCR using five probes whose binding sites are indicated in Supplementary Figure S6. The primer sequences of the probes are described in (16).

To localize endogenous Rio1 to centromeres, the 6Myc-*RIO1* strain and its untagged *RIO1* parent (acting as the negative control) were grown at 24°C and enriched in late G1 with 5 μg/ml α-factor. Cross-linking was done as described above and 6Myc-Rio1 immunoprecipitated with an anti-Myc monoclonal antibody (Covance, Cat # 9E11). The co-immunoprecipitated chromatin was then isolated and amplified with the GenomePlex Complete Whole Genome Amplification Kit (Sigma-Aldrich, Cat # WGA2-10RXN), labeled with biotin-N11-ddATP (1 nM/μl) (NEN) using terminal transferase (Roche, Cat # 03289869103) and hybridized to Affymetrix *S. cerevisiae* Genome Tiling Array 1.0R. The data were analyzed with GeneChip Command Console software (Affymetrix).

ChIP-Sequencing (ChIP-Seq) and data analysis

One to five nanograms of input and chromatin immunoprecipitated DNA were blunt-ended with T4 DNA polymerase (New England Biolabs, Cat # M0203L) and phosphorylated with T4 polynucleotide kinase (New England Biolabs, Cat # M0201L). A single adenine was then added to the 3′-ends using DNA polymerase I Klenow Fragment (3′→5′ exo-) (New England Biolabs, Cat # M0212L) allowing for ligation to an adapter containing a single tyrosine overhang. The ligation products were purified by Agencourt AMPure XP beads (Beckman Coulter, Cat # A63880) and PCR-amplified with PfuUltra II Fusion HS DNA polymerase (Agilent Technologies, Cat # 600674) to enrich fragments with adapters on both ends (Biomek FX, Beckman Coulter). cDNA library concentrations were measured with a Qubit dsDNA HS Assay kit (ThermoFisher Scientific, Cat # 32851) and its size distribution and quality evaluated on a Bioanalyzer 2100 (Agilent Technologies) before cluster generation (FlowCell, Illumina). The libraries were deep sequenced for 50 bases in single-read mode on a HiSeq 2000 sequencing system (Illumina).

Reads were initially filtered (for identification of genomic clusters) or not (for global genomic and mitochondrial clusters) for sacCer3 reference abundant sequences obtained from the Illumina iGenomes support web page (using bowtie version 1.1.1 with default parameters). Next, artefacts were eliminated with Cutadapt v.1.8.3 (50) and reads aligned on the reference genome sacCer3 (46) with Bowtie2 v.2,2,1 software (51) using pre-set end-to-end parameters, while discarding reads with more than one mapping. Duplicate reads were removed with SAMtools rmdup (v.0.1.19) obtaining uniquely mapped reads. After random down-sampling of ChIP-Seq1 aligned reads to the number of ChIP-Seq2 and Input samples using SAMtools, the enriched ChIP-Seq signals were identified using MACS2 v.2.0.10 (52) with the option shift size set to 73 and disabling model and dynamic lambda. The *q*-value threshold was set to 0.005. Data visualizations and gene annotations were carried out using the R package ChIPseeker, the web applications ChIPseek (53) and CEAS (54). The significance of the ChIP-Seq signal cluster distribution across genomic areas and the significance of overlap between clusters of different biological replicates were calculated using the Genomic Association Test (55) python script gat-run, using mappability_36bp.bed as work space file and num-samples = 10000 parameter. The ChIP-Seq maps are available at https://genome.ifom.eu/cgi-bin/hgTracks?db=sacCer3&position=chrXII%3A1-1078177&hgsid=569991_PXM70Mv3Pyng0VlUClaQxpdP7CuY.

Bioinformatic protein-interaction and gene-expression analyses

Interactions were obtained using the web-based version of STRING DB (v.10) (http://string-db.org) (56), setting the 'Active Prediction Methods' to 'experiments' and 'databases' only. Physical or genetic interactions were weighted based on the Y2H *e*-values, the number of times a co-purifying protein was identified and the strength of a genetic growth effect.

The confidence (score) was left at the default setting of medium confidence (0.4) as the extracted combined score was used to weight edge thicknesses. The resulting network was imported into Cytoscape (v. 3.2.1.) (57). Clusters were formed as follows: (i) the MCODE algorithm (58) was used, via the ClusterViz plugin, to determine clusters based on network connectivity (degree threshold:2, k-core threshold:2, Maxdepth:100). (ii) A Gene Ontology (GO) enrichment analysis was then performed in DAVID (59) to establish the dominant functional nature of each network cluster. (iii) A pre-performed global GO analysis (biological processes, cellular components), based on the entire list of 818 significantly regulated genes/transcripts, was then interrogated to extract additional genes related to the function of the cluster. (iv) Clusters were then spatially re-organized using the Allegro spring-electric layout from Allegrolayout (Allegroviva, USA) followed by manual refinement. Nodes were colored by their Log_2 Fold Change value, with values of −4.5 set to red, 0 set to white and +4.5 set to blue. For ease of visualization, the node sizes were also set in proportion to the magnitude of their Log_2 Fold Change values. Edge thicknesses were weighted corresponding to their STRING combined scores. Genes derived from GO terms related to the general description of each cluster were combined to assess enrichment, and related significance of displayed clusters in the networks, with respect to a theoretical human/yeast genome composition.

Creation of Rio1's functional network

To construct the Rio1's functional network we probed our weighted Rio1–protein interaction dataset against our differential gene transcript data against up-to-date yeast protein–protein, yeast protein–transcription factor and yeast protein/transcription factor–gene interaction

data, curated by BIOGRID (60,61), IntAct (62), MINT (63) and TRANSFAC (64). Data integration and significance evaluation were performed with the ResponseNet algorithm, biased toward signaling pathways, as described (65–67). Network layouts were generated with Cytoscape 3.0.1.

Statistical data analysis

Fisher's exact test (hypergeometric data distribution analysis), used to determine non-random associations between two categorical variables, was computed using the Fisher_exact method from SciPy.stats, version 0.19.0. Data averages, standard deviation and standard errors, were calculated with the Excel spreadsheet (Microsoft Office). Statistical significance of independence between datasets ($P < 0.05$, $P < 0.01$ and $P < 0.001$, graphically represented by *, ** and ***, respectively) was calculated using the unpaired, two-tailed student *t*-test (Prism 6.01; GraphPad).

RESULTS

The physical and functional interactome map of Rio1

To determine whether Rio1 is involved in activities beyond regulating rDNA transcription, pre-rRNA processing and 40S small ribosomal subunit maturation, we searched for Rio1 interactors/substrates via yeast two-hybrid (Y2H) interaction screens. To date, only two direct substrates of Rio1 in yeast are known: Rio1 itself (16,68,69) and Rpa43; a conserved subunit of RNA polymerase I (16). To identify protein interactors, we tagged Rio1 N- or C-terminally with either the LexA- or the Gal4 DNA-binding domain. These four bait constructs were then screened three times against all *S. cerevisiae* genes, fused N- or C-terminally to the Gal4 activation domain. Only interactors identified in all three independent screens were retained and provided with a statistical score (*e*-value, explained in the 'Materials and Methods' section), which correlates with the biological significance of the interaction (35–38). The final list of high-confidence hits (*e*-values from 1.0E-02 to 1.0E-24) comprised 97 interactors, including Rio1 itself (15 hits, 7 unique prey fragments, *e*-values = 1.0E-02) (Supplementary Table S1). We previously confirmed that the rDNA helicase Sgs1 identified in the above Y2H screens (3 hits, 1 unique prey fragment, *e*-values = 1.0E-02), co-immunoprecipitates (co-IPs) with and recruits Rio1 to the rDNA (16). To further validate our Y2H dataset we probed an additional three interactors: Rvb2 (28 hits, 2 unique fragments, *e*-values = 1.0E-02), Sky1 (26 hits, 5 unique fragments, *e*-values range from 1.0E-16 to 1.0E-24), Sam37 (11 hits, 5 unique fragments, *e*-values = 1.0E-02) by co-IP analysis. These proteins were selected firstly because they localize to different organelles and contribute to dissimilar activities: Rvb2 is a nuclear ATPase with helicase activity; Sky1 is a nuclear and cytoplasmic protein kinase, while Sam 37 is mitochondrial membrane component (46). Second, because some of these proteins perform multiple roles: Rvb2 contributes to the transcriptional regulation of ribosome biogenesis and ribonucleoprotein complex genes, to the assembly of box C/D snoRNP complexes (70–72) but also promotes RNA polymerase II assembly, DNA damage repair, telomerase complex assembly, mitotic spindle formation, the heat response and phosphatidylinositol three kinase related signaling (71–74), Sky1 regulates mRNA export, cation homeostasis, sulfur metabolism, mitophagy and apoptosis (74–77), while Sam37 is required for mitochondrial protein import (78,79). Third, because the *e*-values of these three interactors cover the entire range of our hit list (1.0E-02 to 1.0E-24; Supplementary Table S1). As shown in Supplementary Figure S1, all three proteins co-IPed with Rio1. Together with the Sgs1-Rio1 co-IP (16), they further validate our Y2H dataset.

Next, our list of 97 proteins was enlarged with 61 Rio1 interactors, reported in the literature (Supplementary Table S2). These included nine proteins identified in Y2H screens ((80), Yeast Resource Center Informatics Platform) and 52 proteins derived from 16 proteomic and biochemical studies (8,9,16,68,81–92). Of the latter, Zuo1; the ribosome-associated chaperone for nascent polypeptide chains, was also identified in our Y2H screens. Next, our 156 unique Rio1 interactors were weighted (see Methods) and functionally clustered (GO term: Biological Process), yielding Rio1's protein–protein interaction map (Figure 1A, enrichment *P*-values are listed in the figure legend). The map exposed Rio1 as a node that integrates eight key activities: ribosome biogenesis and function; cell-cycle regulation; chromosome segregation; physiology; the stress response; transcription, chromatin organization and modification; DNA replication, damage and repair; and metabolism. Using Fisher's exact test (computes the probability that a subpopulation in one sample is over- or under-represented in a second sample beyond what is expected by chance) we compared our 156 interactors against those of 179 other yeast kinases (60). We found that Rio1 integrates sizable subgroups (sharing >10 proteins) of 16 kinase networks (Figure 1B, *P*-values are listed in the figure legend), each of which contributes to a certain cell activity (color-coded as in Figure 1A) (the kinases and their targets are listed in Supplementary Table S3).

Since our list of Rio1 interactors comprised interphase and mitotic proteins, we performed a small-scale genetic study to corroborate its involvement in the cell cycle. By mere luck, while epitope tagging Rio1 (6Myc-Rio1 (16), Rio1-3HA and Rio1-GFP (Supplementary Figure S2B and C)) we found that only the C-terminal 3HA tag negatively affected Rio1 activity, resulting in *RIO1-3HA* behaving like a 'reduced-function' allele. As compared to the *RIO1* control strain, the curtailed activity of Rio1-3HA was evidenced by slow growth (smaller-sized colonies, Supplementary Figure S2B) and by elevated levels of *35S* pre-rRNA transcripts (Supplementary Figure S2A), likely caused by de-repressed transcription and/or reduced processing. In addition, we made a Rio1-overproduction strain by placing endogenous *RIO1* under control of the P_{GAL1} promoter (induced by galactose, repressed by glucose). As expected, *35S* rDNA transcription and/or processing of the *35S* pre-rRNA transcripts were reduced in galactose-containing medium and elevated in the presence of glucose (Supplementary Figure S2A). Next, *RIO1-3HA* and P_{GAL1}-*RIO1* were combined with 20 mutant alleles of proteins mediating key cell-cycle activities (DNA replication, DNA repair, cohesion, condensation, segregation, spindle assembly

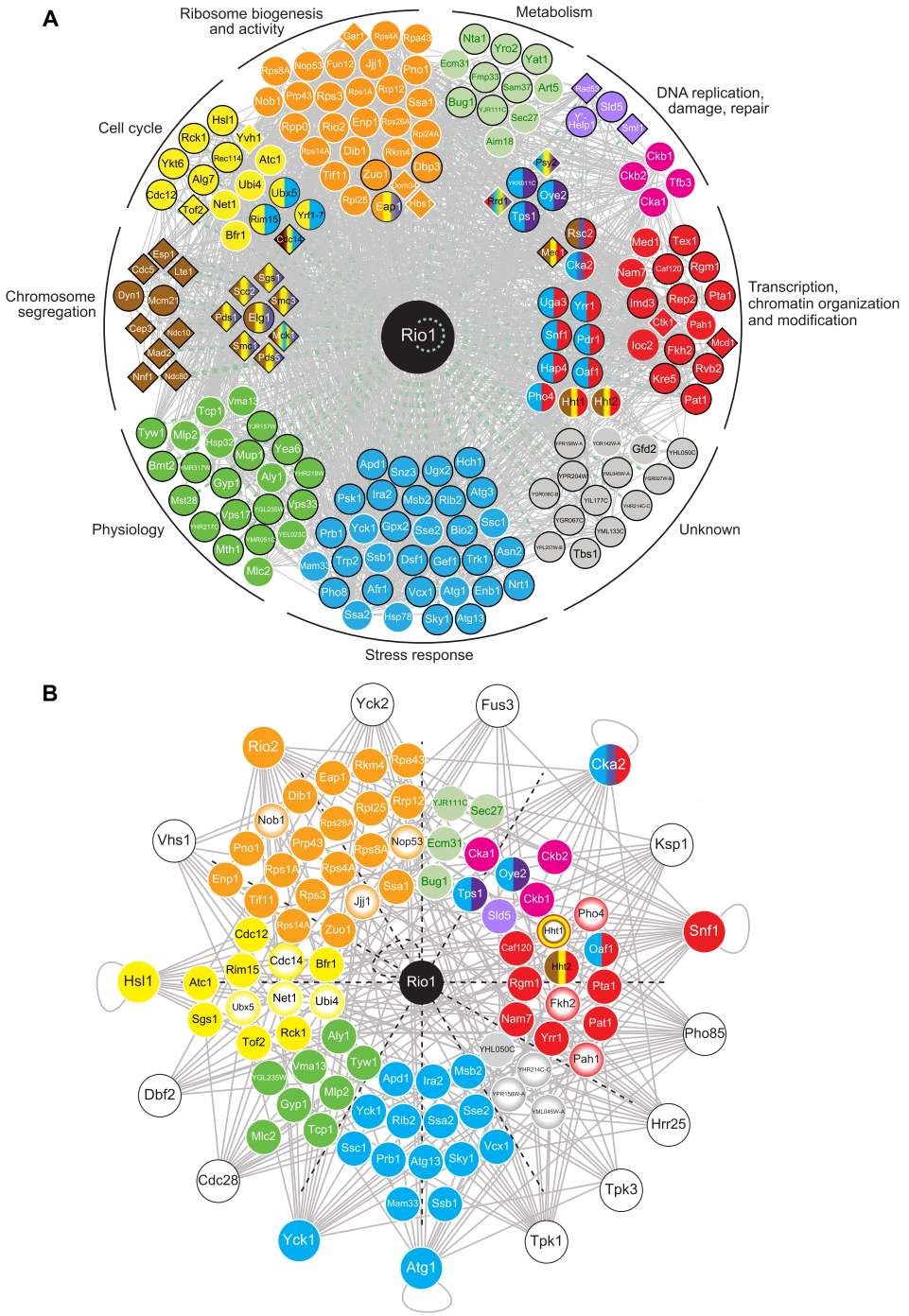

Figure 1. The physical and genetic interaction map of Rio1. (**A**) The Rio1 interactome comprises 184 proteins (156 physical + 28 genetic interactors). Ninty-seven physical interactors were identified in our Y2H screens, nine were retrieved from published (80) and deposited (Yeast Resource Center Informatics Platform, www.yeastrc.org) Y2H screens (black-edged circles). Fifty-two physical interactors were retrieved from published affinity purifications and biochemical studies ((8,9,16,68,81–92), white-edged circles). Rio1 and Zuo1 were identified twice (in our Y2H screens and biochemically (88,91)). Twenty genetic interactors were identified in this study (black-edged diamonds), eight were retrieved from the literature ((12,93–95), white-edged diamonds) (Supplementary Figure S2B and Tables S1, 2 and 4). Each interactor was functionally clustered based on the Gene Ontology term 'Biological Process' associated with it and then color-coded. Proteins belonging to multiple clusters are colored representing each cluster. The *P*-values for functional enrichment were; ribosome biogenesis and activity: 2.1E-10, cell cycle: 1.6E-08; chromosome segregation: 3.7E-08, stress response: 1.8E-10, chromatin organization and modification: 1.2E-01, transcription: 2.4E-03, DNA replication, damage and repair: 5.7E-07. (**B**) Overlap between the Rio1-protein interaction network (includes only its physical interactors) and those of 179 other kinases (60). The 16 top-scoring kinases sharing >10 interacting proteins with Rio1 are shown. Proteins are connected to their master kinase, placed in the outer ring. Shared proteins were functionally clustered and color-coded as in (A). Proteins shared by multiple kinases are shown with a white core. The *P*-values of the overlaps between the Rio1-protein interaction list and those of the other kinases were calculated with Fisher's exact test. They are; Yck2: 4.9E-03, Fus3: 3.5E-04, Cka2: 2.4E-07, Ksp1: 2.9E-03, Snf1: 9.8E-08, Pho85: 6.1E-03, Hrr25: 1.5E-04, Tpk3: 5.3E-04, Tpk1: 3.2E-04, Atg1: 5.5E-04, Yck1: 1.6E-03, Cdc28: 2.5E-02, Dbf2: 4.6E-04, Hsl1: 3.49E-05, Vhs1: 7.3E-06, Rio2: 2.8E-10 (Supplementary Table S3).

checkpoint activity and exit from mitosis). The growth defects of the mutants were either rescued (positive genetic interaction) or exacerbated (negative interaction), indicating that Rio1 antagonizes or supports, respectively, the activity of the investigated protein (Supplementary Figure S2B and Table S4). These data substantiate a functional (and likely also physical) involvement of Rio1 in the activity of the above cell-cycle proteins and processes. Next, four published synthetic genetic screens performed with a heterozygous *rio1Δ* strain extended our map with another eight interaction partners (involved in ribosome biogenesis and translation, metabolism, transcription and cell-cycle regulation) (12,93–95) (Supplementary Table S2). These 28 genetic interactors were added to Rio1's protein-interaction diagram, creating its physical and functional interactome map (Figure 1A).

During our study, Costanzo and colleagues performed a global pair-wise genetic interaction screen to produce the wired diagram of yeast cell function (96). The sub-screen with a temperature-sensitive *rio1* allele identified 142 negative and 125 positive interactors (*P*-values < 0.05, Supplementary Figure S2D). The 267 gene products act across the cell in the processes we had already associated with Rio1 function (Figure 1); including RNA processing (23% of the annotated interactors), cell-cycle activity (21%), ribosome biogenesis (20%), protein folding and turnover (14%), and transcription (13%).

Rio1 localizes to kinetochores

Notwithstanding our positive co-IPs and the full overlay between our physical–genetic interaction map of Rio1, and Rio1's genetic diagram (96), we validated further the involvement of Rio1 in processes and events identified above. Both Costanzo *et al.* and us recognized that Rio1 interacts with the kinetochore, the protein complex that assembles on centromeres to orchestrate chromosome segregation (kinetochore subunit Mcm21 as a Y2H partner, 12 alleles encoding kinetochore components that strongly genetically interacted with Rio1). To examine whether Rio1 actually localizes to kinetochores, we immunoprecipitated 6Myc-Rio1 from crosslinked G1 cells (enriched at START with the α-factor pheromone) using a monoclonal anti-Myc antibody (the untagged *RIO1* strain acted as the negative control) and submitted the chromatin co-immunoprecipitating with 6Myc-Rio1 to genome hybridization analysis (ChIP-chip). We localized 6Myc-Rio1 at kinetochores (representative signals at CEN5 and CEN10 are shown in Figure 2A) while the protein was not identified at kinetochores in the untagged strain. To further corroborate its presence at kinetochores, we localized 6Myc-Rio1 by IF microscopy of spread nuclei isolated from cells enriched in G1 (cell cycle stage in which all kinetochores are clustered near the spindle pole). Next to localizing 6Myc-Rio1 to the nucleolus (rDNA, positive control; Nop1 as the nucleolar marker) we also identified the protein at kinetochores (kinetochore subunit Ndc80 as the marker) (Figure 2B). Combined, its presence at kinetochores underscores a contribution of Rio1 to kinetochore activity and consequently to chromosome transmission. This observation helps to explain why a reduced-activity *rio1* mutant suffers from elevated chromosome loss and metaphase delay (88).

Rio1 promotes rDNA replication

Heterozygous *rio1Δ* mutants are sensitive to drugs obstructing DNA replication (20). This phenotype indicates an involvement of Rio1 in the process, a hypothesis that is supported by both its physical and genetic interactions with proteins mediating DNA replication (Figure 1A; Supplementary Figure S2B and Table S1, (96)). To verify its contribution, we wished to probe replication fork activity at the rDNA (at which Rio1 accumulates (16)), in wild-type yeast and in yeast lacking Rio1. However, since Rio1 activity is essential for viability, we had to conditionally eliminate the protein and chose the auxin-inducible degron (AID) system for that (34). After tagging Rio1 at its C-terminus with the AID degron cassette (hence producing the *RIO1-AID*, P_{ADH1}-*OsTIR1-9Myc* strain; hereafter named *RIO1-AID*), we probed Rio1-AID protein activity and confirmed it was identical to that exhibited by Rio1 in the untagged parent strain. Indeed, growth assays did not reveal any negative effect on fitness or growth rate (colony size, Supplementary Figure S3A) and *35S* pre-rRNA transcript levels were also identical to those measured in the *RIO1* stain (Supplementary Figure S3B). Next, we assayed the Rio1-AID degradation kinetics. Within 30 min of adding 500 μM of auxin to the *RIO1-AID* culture, Rio1-AID became undetectable by western blot hybridization analysis (Supplementary Figure S3C). Its depletion was supported by an increase in *35S* pre-rRNA transcript levels (Supplementary Figure S3B). Because of its key roles in *35S* rDNA transcription, pre-rRNA processing and 40S small ribosomal particle maturation, we examined whether depleting Rio1-AID for 1h affected ribosome biogenesis and translation activity. Specifically, the wild-type and *RIO1-AID* strains were treated for 1 h with 500 μM of auxin. Whole-cell extracts were then made and ran through a sucrose gradient to profile the 40S and 60S ribosomal subunits, the mature 80S monosomes and the translationally active polysomes. A minor reduction in 40S and a slight increase in 60S ribosomal subunits was observed (Supplementary Figure S3D). When we treated the cells with 4TU to label the newly synthesized (r)RNAs, 40 min into auxin treatment, we detected an increase in 20S pre-rRNA levels, reflecting reduced Rio1 activity in the cell (Supplementary Figure S3E). However, despite the mild 40S biogenesis defect, the ratio between the concentration of 80S monosomes and polysomes was similar in the wild-type and Rio1-AID-depleted strains (5.2 versus 5.6, respectively), suggesting that cellular translation activity was not significantly affected. Indeed, a short methyl-3H-methionine pulse revealed no differences in the levels of radiolabeled, neo-synthesized proteins that were produced in both strains (Supplementary Figure S3F). This finding implies that any phenotype observed in yeast depleted of Rio1 for only 1 h is not caused by pleiotropic effects due to reduced intracellular protein synthesis but rather by the absence of Rio1 activity in the process being studied.

To finally assay DNA replication at the rDNA and control ARS305 sequence in the presence and absence of Rio1 activity, we synchronized the *RIO1-AID* cells in late G1

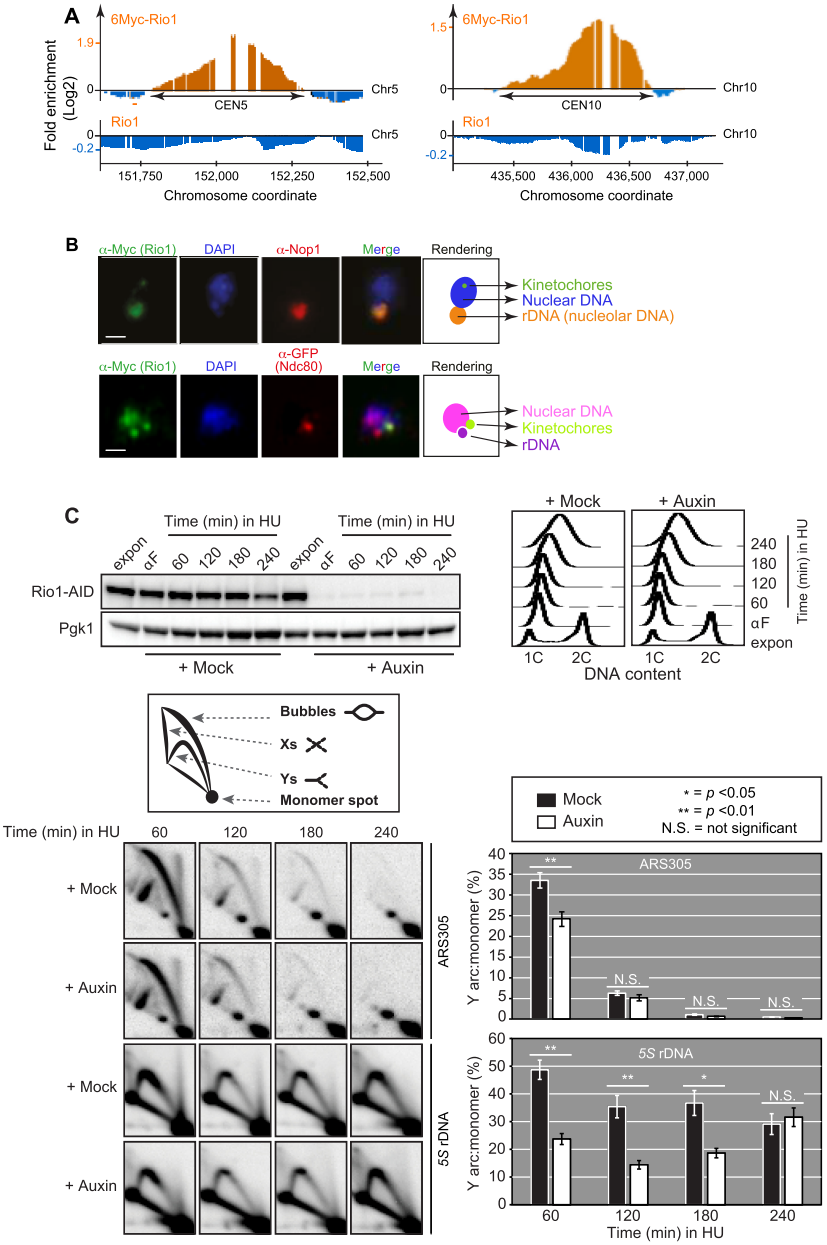

Figure 2. Rio1 localizes to kinetochores and promotes replication fork velocity/stability at the rDNA. (**A**) To probe the localization of Rio1 to kinetochores, we submitted a strain endogenously expressing *6Myc-RIO1* and its untagged parent to anti-Myc based chromatin immunoprecipitation, followed by microarray hybridization (ChIP-chip). The hybridization profiles (orange) at CEN5 and CEN10 are shown. (**B**) To corroborate the localization of Rio1 to kinetochores by microscopy, we isolated the nuclei from G1 cells (all 16 kinetochores are concentrated near the spindle pole) and then spread, washed and submitted them to indirect IF analysis. We identified Rio1 at both the rDNA (Nop1 as the rDNA/nucleolar marker) and at kinetochores (Ndc80 as the marker). DAPI strongly dyes the chromosomes but not the nucleolus as the latter is highly enriched with proteins, preventing DAPI from staining the rDNA. Scale bar = 5 μm. (**C**) To evaluate the contribution of Rio1 activity to chromosome replication we analyzed replication intermediates at the rDNA array and at negative control ARS305 in HU-treated *RIO1-AID, P_{ADH1}-OsTIR1-9Myc* cells (next named *RIO1-AID*) that contained or were depleted of Rio1 activity. The *RIO1-AID* strain was grown exponentially (expon), then synchronized in G1 with α-factor (αF) and finally released into the cell cycle using 200 mM HU-containing YPD medium supplemented with 500 μM of auxin or mock solution. Samples were collected at the indicated time points. Rio1-AID depletion was evidenced by anti-AID western blot hybridization (3-phosphoglycerate kinase Pgk1 acted as the loading control) (upper left blots). Cell-cycle progression was tracked by FACS-based analysis of DNA content (upper right plots). After releasing the cells from G1, genomic DNA was extracted from culture samples taken at the indicated time point (60, 120, 180 and 240 min) and treated with the restriction endonucleases EcoRV and HindIII to analyze ARS305, or with BglII to analyze *5S* rDNA. Following 2D agarose gel electrophoresis, replication intermediates accumulating at both sites were visualized by Southern blot hybridization. The topologies of replication intermediates potentially accumulating in the presence of HU are drawn. The bottom left radiographs show the Southern hybridization images depicting replication fork intermediates at ARS305 and *5S* rDNA in *RIO1-AID* cells exposed to HU and treated with 500 μM of auxin or mock solution. Results of a representative experiment are shown. The bottom right graphs show the relative values of the Y-arc signals quantitated against those of the monomer spots. The number of unidirectional Y-arc replication intermediates was consistently reduced at the rDNA locus in the Rio1-depleted cells. Error bars = standard deviation. The data were calculated from four (rDNA) or five (ARS305) independent experiments. Statistical (in)significance of independence between the mock- and auxin-treated datasets ($P < 0.05$ (*) and $P < 0.01$ (**), N.S. = insignificant data independence) was calculated using the unpaired, two-tailed student *t*-test.

with α-factor. The cells were then released into the cell cycle using YPD medium, supplemented with 500 μM of auxin or a mock solution and with 200 mM of HU to halt DNA replication. After confirming Rio1-AID depletion (western blot hybridization) and interphase arrest by the S-phase checkpoint (FACS analysis) (Figure 2C), we performed 2D agarose gel electrophoresis followed by Southern blot hybridization analysis using anti-rDNA and anti-ARS305 probes. Four (rDNA) or five (ARS305) independent experiments were performed for each condition (auxin and mock treatment). Examination of the replication fork intermediates revealed a significant reduction in unidirectional replication forks (Y arcs) at the rDNA, as compared to the ARS305 sequence, in the Rio1-depleted cells challenged with HU (Figure 2C). This observation underscores a supportive role for Rio1 in rDNA replication by regulating local replication fork velocity and stability. This contribution of Rio1 complements its interaction with the rDNA helicase Sgs1 and its repression of rDNA transcription during S-phase (16) in order to avoid clashes between the replisome and RNA polymerase I, which trigger the genetic instability of this essential repeat region.

Establishing Rio1's transcriptome map

Our Rio1-protein interaction list contained histone H3 proteins Hht1 and Hht2, transcription factors, and proteins implicated in chromatin assembly, modification and remodeling. In addition, Costanzo *et al.* identified 29 *rio1*-interacting genes (14 negative, 15 positive) whose proteins regulate gene transcription. These findings and the fact that Rio1 regulates rDNA transcription by RNA polymerase I (16) convinced us to probe whether the enzyme controls gene expression beyond the rDNA as well. As such, six *RIO1-AID* cultures were grown exponentially in rich medium (YPD). Three of them were then treated for 1 h with 500 μM of auxin, the other three with a mock solution. A 1-h depletion was chosen because it allows for the removal of Rio1 without affecting global translation activity (see above). This window also permits for a solid response at the transcriptional level. Next, total RNA was isolated from the cells. The nuclear and mitochondrial rRNAs were removed (representing >95% of the yeast transcripts) to expose the less abundant RNAs, which were reverse transcribed and deep sequenced (RNA-Seq). After averaging and filtering the triple datasets (RPKM [reads per kilobase of transcript per million reads mapped] >1), transcript levels of 818 genes (nuclear + mitochondrial) emerged as being differentially changed in yeast depleted of Rio1 (P-value ≤ 0.05) (Supplementary Figures S4 and 5A–C; Supplementary Table S5). While its impact on gene expression/transcript levels ranged from 11-fold increase (*RPL7B*) to 18-fold reduction (*YDR215C*), Rio1 upregulated most (66%) of its target genes (Supplementary Figure S5C). We underline that the measured changes in transcript levels produced from the 818 identified ORFs can be the consequence not only of changes in gene expression but also of altered transcript decay and stability due to the lack of Rio1 activity.

Next, we assessed the functionality of the 818 genes via GO enrichment analysis (P-values are tabulated in Supplementary Table S6). We then color- and size-weighted the impact that Rio1 has on the transcript levels of each gene. The 548 genes/transcripts that are upregulated by Rio1 activity are colored red, while the 270 genes/transcripts that are downregulated by Rio1 activity are depicted in blue (Figure 3).

Our study revealed, first and foremost, that Rio1 upregulates the transcript levels of all RP genes (RP regulon) and of the RP transcriptional activator Rap1 (Supplementary Table S5). Since Rio1 is a Ribi member, we did not anticipate it to regulate the RP regulon, possibly by controlling *RAP1* expression (Supplementary Figure S11B). Also, Rio1 modulates the transcriptome state of 20% of the Ribi regulon (18,19) hence additionally regulating ribosome biogenesis (e.g. subunits of the rRNA-processing SSU processome, ribosome chaperones, transporters, etc.) and activity (translation initiation factors, aminoacyl-tRNA synthetases, etc.) through Ribi gene expression. We underscore that the significant changes observed in RP and Ribi transcript levels measured after 1 h of Rio1-AID depletion are fully compatible with the cells being translationally competent since the ribosomes that were synthesized before and hence were active during the 1h-depletion window, ensured bulk protein synthesis at normal capacity (Supplementary Figure S3F).

Second, Rio1 reduces the levels of transcripts derived from the genes encoding all 26S proteasome components (including its ATPases and the ubiquitin-specific protease Ubp6) and of the gene coding for proteasomal transcription factor Rpn4. As such, Rio1 can control protein degradation/inactivation in the cell. Noteworthy, proteasome expression opposes that of the RPs, indicating that when protein synthesis is required, Rio1 may downregulate proteasome expression (and *vice versa*). Also, Rio1 affects the transcript levels of an assortment of chaperones, emphasizing its protagonist role in managing protein levels, quality and activity.

Third; carbon and amino acid biosynthesis, purine, pyrimidine, phosphorous and lipid biosynthetic pathways, as well as ATP synthesis and/or hydrolysis are subject to regulation by Rio1.

Fourth, Rio1 regulates the mRNA levels of chromatin assembly and remodeling factors, cytoskeleton components and regulators, cell wall biogenesis enzymes, cell cycle determinants and proteins mediating exo- and endocytosis.

Our transcriptome data further show that Rio1 not only physically interacts with a large number of proteins but also regulates the expression of 29 of them (listed in Supplementary Table S7), including regulators such as the kinase Sky1, vacuolar proteinase Prb1, various protein chaperones, histone H3 proteins Hht1 and Hht2, translational initiation factor eIF4A -via which the 40S ribosomal subunit scans for the start codon-, RPs and metabolic enzymes. As such, Rio1 seems to orchestrate intracellular activities both at the protein and chromatin/RNA levels.

Establishing Rio1's chromatin interaction map

After disclosing its transcriptome, we examined to which extent Rio1 regulates its target genes by localizing to promoters and/or coding sequences, by acting in off-DNA fashion on transcription factors, RNA polymerases or chro-

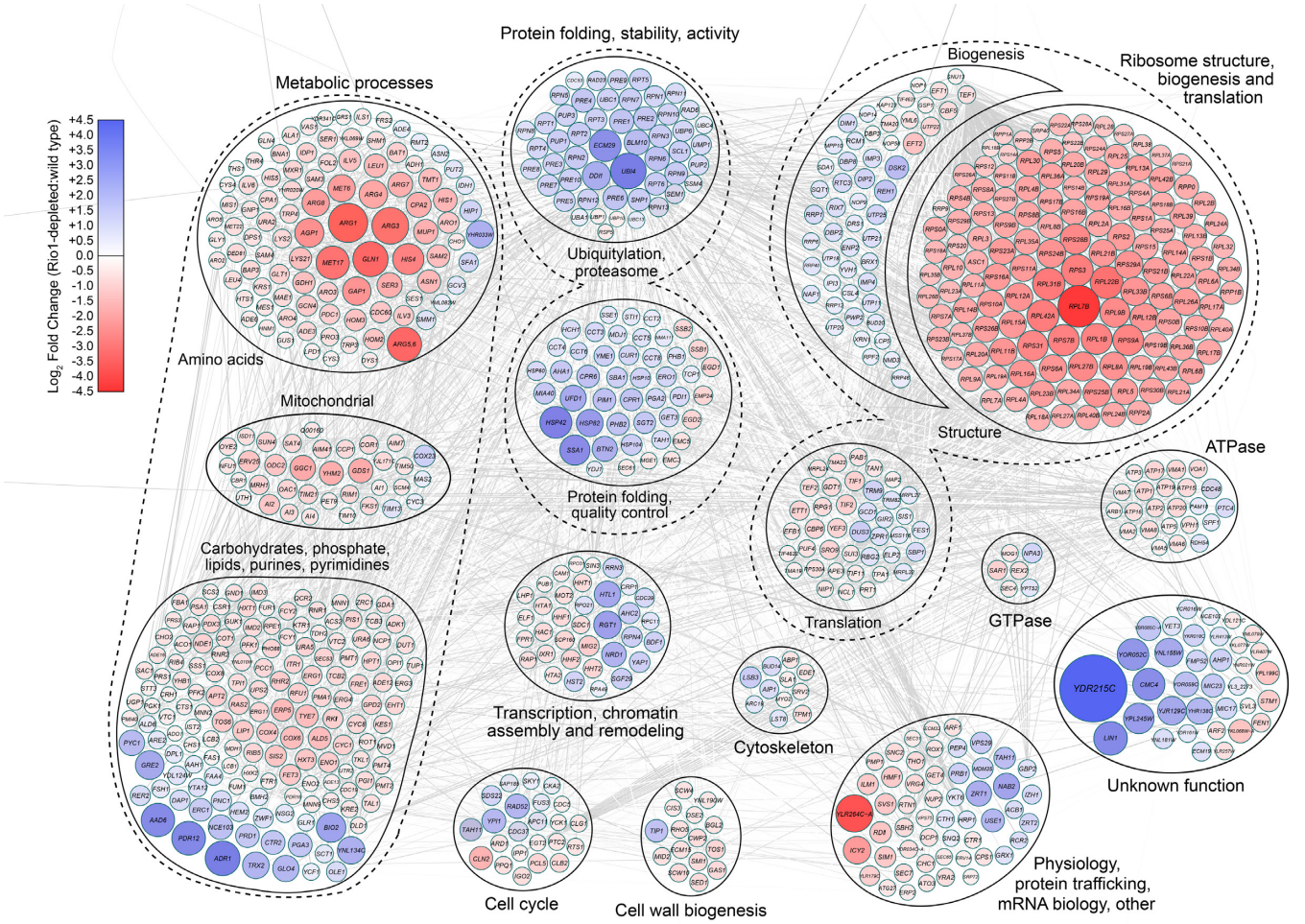

Figure 3. The Rio1 transcriptome map. The 818 genes whose transcript levels were found to have differentially changed in yeast depleted of Rio1 (as compared to the *RIO1-AID* strain not depleted of Rio1), were functionally clustered based on the Gene Ontology term 'Biological Process' associated with each gene (enrichment *P*-values are listed in Supplementary Table S6). The differential state of each transcript is indicated by symbol size and color intensity (see gradient on the left). Genes whose transcript levels increased due to Rio1 activity are shown in red whereas those whose levels decreased due to Rio1 activity are indicated in blue. The gray lines in the background represent all known interactions between the 818 gene products, as cataloged in protein interaction databases.

matin remodelers/modifiers, or by affecting RNA turnover or stability (Figure 1A, Supplementary Tables S1 and 2). As such, three *RIO1-AID* cultures were exponentially grown in rich medium (YPD, same conditions as for the RNA-Seq experiments, allowing us to correlate both datasets). The cells were then submitted to ChIP analysis with a monoclonal anti-AID antibody, and the generated DNA libraries deep-sequenced (ChIP-Seq). In three parallel negative control experiments, *RIO1-AID* cultures were subjected to the ChIP protocol that did not employ the anti-AID antibody, while untagged *RIO1* cultures were submitted to ChIP experiments that did and did not use the anti-AID antibody. RT-qPCR analysis of the rDNA sequence, to which Rio1 localizes, indicated the absence of background noise in our Rio1-AID ChIP experiments (Supplementary Figure S6). Examination of the anti-AID ChIP-sequencing data derived from the three *RIO1-AID* cultures revealed a preponderance of reads originating from the mitochondrial chromosome (present in 20–50 copies per haploid cell), obscuring the signals derived from the nuclear chromatin. After separating the mitochondrial chromatin reads, we distinguished 297, 397 and 481 Rio1-binding sites across the nuclear genome, respectively, of which 125 sites were consistently identified in all three experiments (Supplementary Figure S7A-B and Table S8). Along the nuclear DNA, Rio1 was enriched at promoter regions (10.5 ± 0.5%), coding sequences (69 ± 2%) and near transcription termination sites (10 ± 2.0%) (Supplementary Figure S7C). As for the Rio1-controlled genes identified by RNA-Seq: in at least 2 of the 3 ChIP experiments we found that 10 harbored a Rio1-binding signal in their promoters, 12 in their coding sequences, while 1 gene (*SSA1*) had Rio1 bound to its promoter and coding sequence (these 23 genes are indicated in bold italic font in Figure 4A, examples are shown in Figure 4B). In one of the three ChIP-Seq experiments, we captured Rio1 at the promoter or coding sequence of an additional 29 Rio1-controlled genes (italic font in Figure 4A), suggesting short-lived interactions between Rio1 and these genes. With the exception of these 52 transcriptome members and the rDNA (Figure 4C and Supplementary Fig-

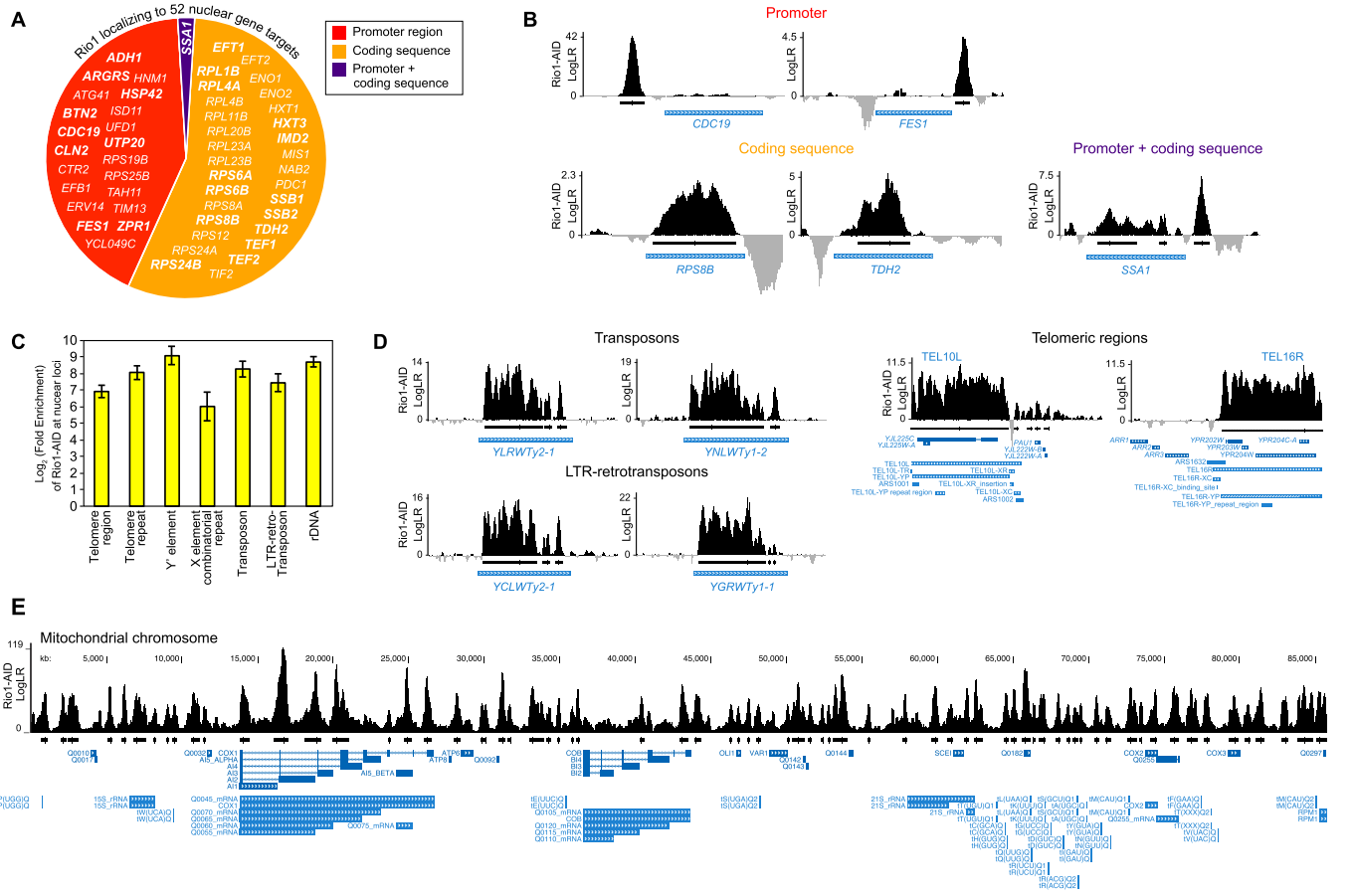

Figure 4. The Rio1-chromatin binding map. (**A**) Fifty-two nuclear genes whose expressions are under the direct regulation of Rio1 and which harbor its footprint in their promoter regions (red segment), coding sequences (orange segment) or both (purple segment). The genes indicated in bold italic font contained a high-scoring Rio1 signal in at least two independent ChIP-Seq experiments. The genes indicated in italic font contained a high-scoring Rio1 signal in singular ChIP-Seq experiments. (**B**) Visual representations of Rio1 localizing to target genes at their promoter sequence (*CDC19*, *FES1*), coding sequence (*RPS8B*, *TDH2*) or both (*SSA1*). The LogLR (likelihood ratio) values for the local enrichment of Rio1 relative to the input are shown. The black marks underneath each Rio1 signal indicate the part of the footprint that is significant (q-value ≤ 0.005). (**C**) Enrichment of Rio1 at specific nuclear regions and loci. The data represent the average values measured in three independent ChIP-Seq experiments. Error bars = standard errors. (**D**) Visual representations of Rio1 localizing to transposons (*YLRWTy2-1*, *YNLWTy1-2*), LTR-retrotransposons (*YCLWTy2-1*, *YGRWTy1-1*) and telomere regions (*TEL10L*, *TEL16R*). (**E**) Visual representation of Rio1 associating with the mitochondrial genome.

ure S7E) Rio1 transcriptionally regulates the majority of its ORFs (94%) either in an indirect, off-DNA fashion or directly at the chromatin through short-lived physical interactions. Both observations are consistent with activity models established for other protein kinases that regulate gene transcription, including the yeast and human mitogen-activated protein kinases (97). Rio1 footprints were also distinguished across the chromatin landscape (Supplementary Table S8). Of the 297, 397 and 481 Rio1-binding sites that were identified across the nuclear genome in our repeat experiments, we found that 82 ± 2% of them did not affect transcript levels of the nearby ORF when Rio1 was depleted. A lack of association at the transcriptional level may indicate roles of Rio1 in basic chromatin activities (98–100). Indeed, Rio1 co-purified with histone H3 proteins Hht1 and Hht2 (85) and physically and genetically interacted with DNA helicases, repair enzymes, DNA replication regulators, cohesin, condensin and the chromosome-segregating centromere and kinetochore proteins (Figure 1; Supplementary Figure S2B and D). For example, Rio1 was identified at all 32 telomeres and telomere repeat sequences (Figure 4C and D) and at transposable gene elements (Figure 4C and D). Activities at these regions control genetic stability, chromosome length and cellular lifespan; as well as stress adaptation via transposition-mediated gene regulation, respectively. In contrast, the lack of Rio1 footprints at genes whose transcripts are significantly affected by the absence of Rio1 activity may indicate fast kinetics at the chromatin levels (Rio1 not captured) but also point to an involvement of Rio1 in RNA processing, turnover and stability.

Next, analysis of the mitochondrial ChIP-Seq reads identified Rio1 along the mitochondrial DNA (Figure 4E) consistent with regulating seven of its encoded messages (Figure 3; ChIP-Seq1-3 P-values = 5.0E-14, 1.0E-71 and 4.4E-48, respectively). Rio1-AID signals were prominent at the *15S* rDNA and *21S* rDNA promoter and transcribed regions. Our RNA-Seq experiments had revealed that Rio1 promotes *21S* rDNA expression. The *21S* pre-rRNA self-splices to produce the mature *21S* rRNA, which together with the *15S* rRNA becomes part of the mitochondrial ri-

bosomes (101). The mitochondrial ChIP-Seq data extended the tally of genes that are under the direct control of Rio1 to at least 59 (52 nuclear + 7 mitochondrial). We emphasize that Rio1 regulates the transcription of both the nuclear and mitochondrial rDNA genes.

Rio1 localizes to the nucleus, cytosol, mitochondria and vacuoles

Our Rio1-protein, gene-transcription and genome-binding maps, as well its global genetic interaction diagram (96) indicate that Rio1 acts and localizes throughout the cell. Indirect IF widefield imaging of isolated nuclei previously distinguished Rio1 at the nucleus and the nucleolus (16). IF imaging of whole yeast cells endogenously expressing Rio1-GFP (the GFP tag did not affect cell fitness, Supplementary Figure S2C) identified the protein at the nucleus (DAPI weakly stains the nucleolus due to its high protein content) and the cytoplasm (compatible with Rio1 contributing to 40S maturation). No anti-GFP IF signals were identified in the *RIO1* strain.

To localize Rio1 with ultrastructural resolution, we submitted the *RIO1-GFP* strain to anti-GFP cryo-immunogold EM (Figure 5B; the untagged *RIO1* strain acted as the negative control, Supplementary Figure S8). The efficiency with which the GFP epitope was identified by the anti-GFP antibody and gold-labeled protein A, was determined by the method of Griffiths (41) as 10% (standard of excellence), meaning that one gold signal represents 10 Rio1-GFP molecules. We distinguished Rio1-GFP in the nucleus (20-fold enrichment over the negative control), the cytosol (3-fold enrichment), mitochondria (lumen + membrane, 53-fold enrichment) and the vacuole (lumen + membrane, 75-fold enrichment). While it is difficult to compare IF imaging (Rio1 signals throughout the cytosol) and EM, we believe that the less-than-expected 3-fold enrichment of Rio1-GFP signals in the cytoplasm as observed by EM is due to poor gold (10 nm)-immune-complex formation of Rio1-GFP bound to the pre-ribosomes (steric hindrance).

The identification and enrichment of Rio1-GFP at mitochondria is consistent with its localization to the mitochondrial genome, as observed in our ChIP-Seq experiments (Figure 4E). Furthermore, as determined with MitoFates software (102), Rio1 contains a putative N-terminal mitochondrial pre-sequence MPP processing site (residues 41–50, predicted cleavage at residue 42) and a consensus Tom20 recognition motif (residues 90–95), which is compulsory for mitochondrial import. Rio1 physically interacts with mitochondrial membrane protein Sam37 (Figure 1A and Supplementary Figure S1) and with 37 other mitochondrial proteins (Supplementary Tables S1 and 2). Besides regulating the expression of seven mitochondrial ORFs, Rio1 is poised to act in mitochondrial (oxidative) signaling as it further determines the transcription of 123 nuclear genes whose proteins catalyze mitochondrial activities including metabolic, energy generating, calcium buffering, stress signaling and apoptotic mitochondrial processes (103,104) (Supplementary Table S5).

The localization of Rio1 to the vacuole; the storage and recycling organelle that mediates the cellular adaptation to nutrient deprivation, osmotic shock and ionic stress (105,106), is consistent with Rio1 physically interacting with nine proteins involved in vacuolar fusion, vacuolar protease and phosphatase activity, vacuolar import and export, and the cytoplasm-to-vacuole targeting pathway (Figure 1A; Supplementary Tables S1 and 2). A functional connection between Rio1 and vacuole biology is reinforced by Rio1 regulating the expression of 32 genes involved in vacuolar processes (Supplementary Table S5), including two genes whose protein products interact with Rio1 at vacuoles (vacuolar proteinase PrB1, v-SNARE vacuolar membrane protein Ykt6). In summary, our intracellular imaging data infer that Rio1 not only acts in the nucleus, nucleolus and the cytosol (as reported before), but also at mitochondria and the vacuole. The presence and activity of Rio1 at these organelles is supported by its global genetic diagram (Supplementary Figure S2D ((96)) and our interactome, transcriptome and chromatin-binding maps.

Establishing the activity network of Rio1

While our findings expanded the functional spectrum of Rio1, the question became: how are Rio1, its gene/transcript and protein targets—localizing throughout the cell—functionally and physically connected? Indeed, Rio1 regulates its downstream processes largely by employing partner regulators (enzymes, transcription factors, etc.). Answering this question required the identification of intermediary 'nodes', including transcription factors known to directly act at the ORFs here identified based on the changes measured in their transcript levels, as Rio1 gene targets. To accomplish this task, we collected all up-to-date, experimentally validated yeast protein–protein, yeast protein–transcription factor, yeast protein–gene and transcription factor–gene interactions, as curated by BIOGRID (60,61), IntAct (62), MINT (63) and TRANSFAC (64). Each of the 119 600 protein–protein and 14 010 protein/transcription factor–DNA contacts (represented by 6237 proteins; including 217 transcription factors) was then weighted via a Bayesian scheme to add statistical relevance to each interaction. Next, the ResponseNet algorithm (65–67) (freely accessible at http://netbio.bgu.ac.il/respnet/) implemented a maximum-probability, minimum-cost flow optimization approach to combine our own interaction and gene-expression data into the above catalogs to produce a top-to-bottom (Rio1-to-genes) signaling network (Supplementary Figure S9). Using this network, one can step backward from a chosen gene target to identify the upstream protein contacts (including functional nodes identified by the algorithm from the interaction catalogs) that link Rio1 to the gene. ResponseNet correctly identified protein kinase Ck2 (subunits Cka1 and Cka2) as a Rio1 activator, as reported (68) (Figure 6). The algorithm also identified seven transcription factors, with which Rio1 physically interacts (six identified in our Y2H screens, one was co-purified with Rio1 (83); indicated by yellow triangles in Figure 6). These transcription factors functionally associate Rio1 with 47 target genes (blue squares). Rio1-target genes such as *GCN4, RPN4* and *RAP1* encode key node transcriptional regulators that modulate the expression of metabolic proteins, the 26S proteasome subunits, and the structural

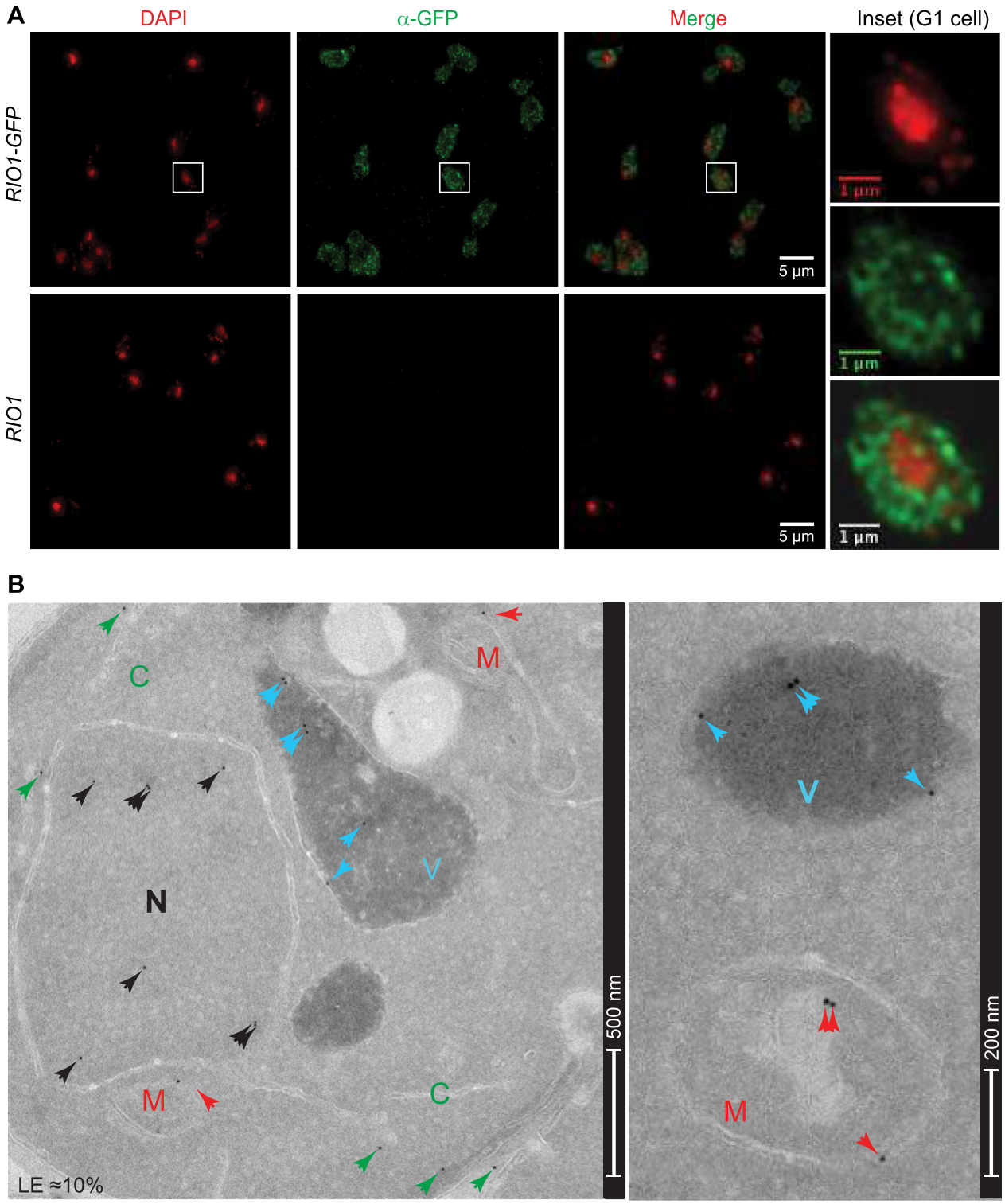

Figure 5. Rio1 localizes to the nucleus, cytosol, vacuoles and mitochondria. (**A**) Indirect wide-field IF imaging of endogenous Rio1-GFP localization in exponentially growing *Saccharomyces cerevisiae*. The untagged parent (*RIO1*) was analyzed as the negative control. Imaging was performed with Living Colours Full-Length anti-GFP polyclonal rabbit antibody and FITC-conjugated anti-rabbit secondary antibody. Rio1-GFP signals are shown in green. DAPI stains the nuclear DNA (red) and not the nucleolar rDNA since the high levels of nucleolar proteins prevent DAPI from intercalating into the rDNA array. The right images show zoom-ins of the inset G1 cell. (**B**) Cryo-immunogold EM images of exponentially grown yeast cells endogenously expressing Rio1-GFP. Single slices of gelatin-embedded yeast (50–60 nm thickness) were incubated with rabbit anti-GFP antibody and gold (10 nm)-labeled protein A, and then imaged. Rio1 was identified at the nucleus (N, black arrows), at the vacuolar lumen and membrane (V, blue arrows), at mitochondria (M, red arrows) and in the cytosol (C, green arrows). The labeling efficiency (LE) ≈ 10% (standard of excellence, quantitated using the method of Griffiths (41), means that one gold signal corresponds to 10 Rio1-GFP molecules. A negative control image of the untagged *RIO1* strain and statistical analysis of Rio1 localization in the *RIO1* and *RIO1-GFP* strains are shown in Supplementary Figure S8A and B, respectively.

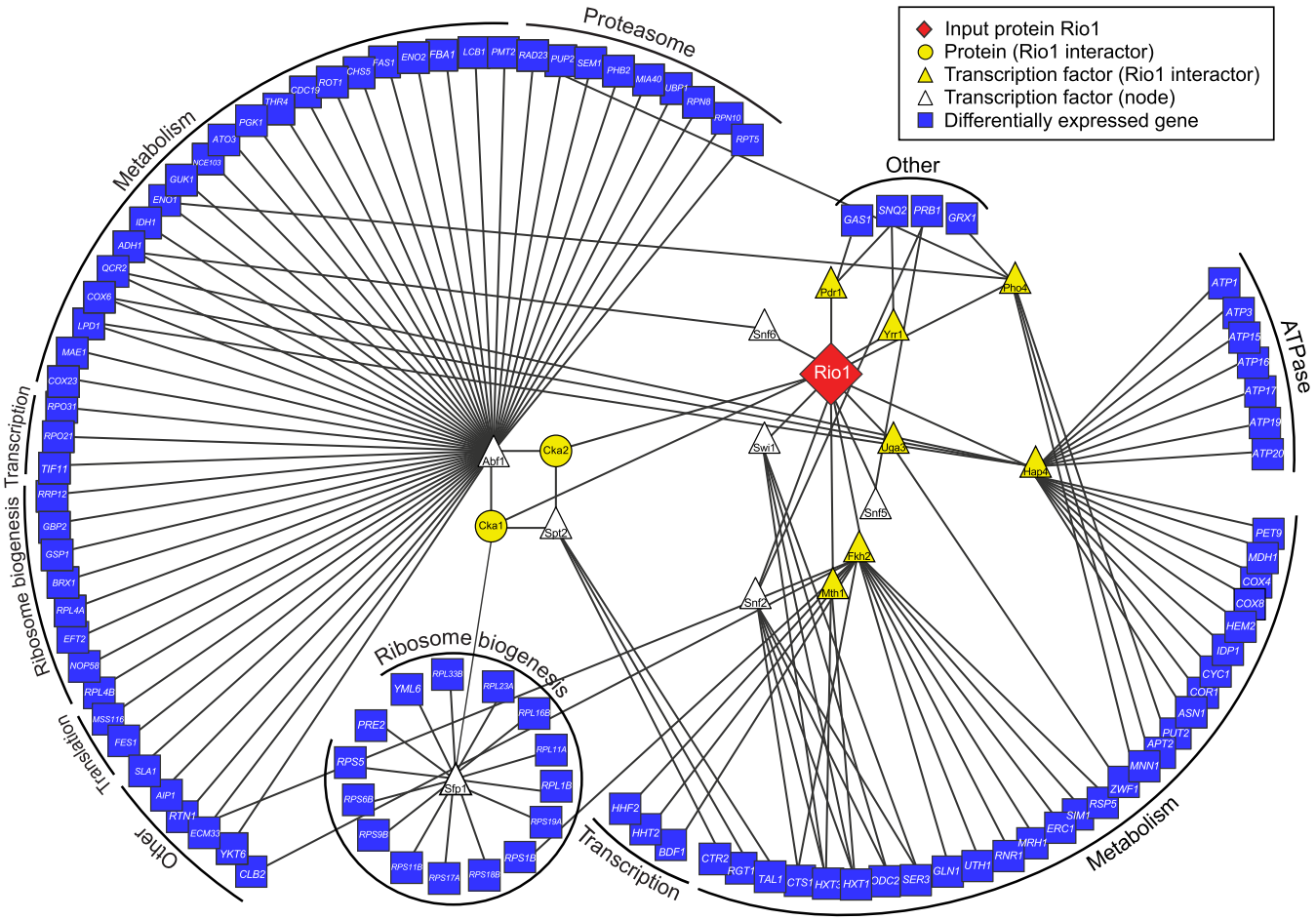

Figure 6. The Rio1-Ck2 sub-network in *Saccharomyces cerevisiae.* The Rio1-Ck2 sub-network, which is part of Rio1's global network (depicted in Supplementary Figure S9), comprises 106 differentially expressed genes (blue squares), 14 transcription factors; 7 of which physically interact with Rio1 (yellow triangles), while 7 were identified by the algorithm as intermediate nodes (white triangles). The two subunits of the protein kinase Ck2 (Cka1, Cka2), which physically interacts with Rio1 (68), are indicated by yellow circles.

ribosomal subunits plus metabolic proteins, respectively (Supplementary Figures S10 and 11). By integrating a large collection of similar sub-networks, Rio1 can conduct its activities on a global level.

Our network analysis also highlights its multi-layered regulation by Rio1. First, Rio1 acts at the protein, gene and RNA levels (many of its physical interactors and gene targets are involved in RNA synthesis, pre-RNA processing, and regulation of mRNA decay). Second, 29 Rio1 gene targets encode proteins that in turn physically interact with Rio1 (listed in Supplementary Table S7). Third, eight transcription factors whose expression states are controlled by Rio1 (Gcn4, Mig2, Mot2, Rap1, Rlm1, Rox1, Rpn4 and Tup1) in turn modulate the expression of numerous Rio1-controlled genes, indicating that the Rio1 network is feedback regulated. Using our network one can experimentally assess how and/or via which partners Rio1 modulates a certain protein/gene/RNA or cellular activity.

Rio1 and its network respond to nutritional availability

Having mapped how Rio1, its interactors and gene targets are connected within its signaling network, we wondered which circumstance(s) would provoke Rio1 to act upon it. While Rio1 is a member of the Ribi regulon, which strongly responds to nutrient availability, we wondered whether its network is linked also to other cues. Hence we used Fisher's exact test to compare Rio1's transcriptome dataset with those of other regulatory networks in yeast. We found that the Rio1 gene regulon significantly overlapped with those of the heat (P-value = 1.4E-07), osmotic (P-value = 3.7E-56), nutritional (P-value = 7.2E-22) and oxidative (P-value = 7.3E-04) stress-response systems (107–111) (the transcriptomes are size-weighted in Figure 7A, individual genes are listed in Supplementary Table S10). This observation suggested that Rio1 and its network are physically and functionally integrated with these response networks. In addition, Rio1 might relay multiple cues into its system, allowing yeast to respond to a number of growth conditions. Given that the Rio1 regulon is highly enriched in genes coding for ribosome biogenesis and activity, we probed whether the overlap between the Rio1 and stress response regulons is simply due to their shared regulation of ribosome biology. When we removed ribosome-linked genes from all regulons and reanalyzed their overlap with the Rio1 regulon devoid of genes mediating ribosome formation and activity,

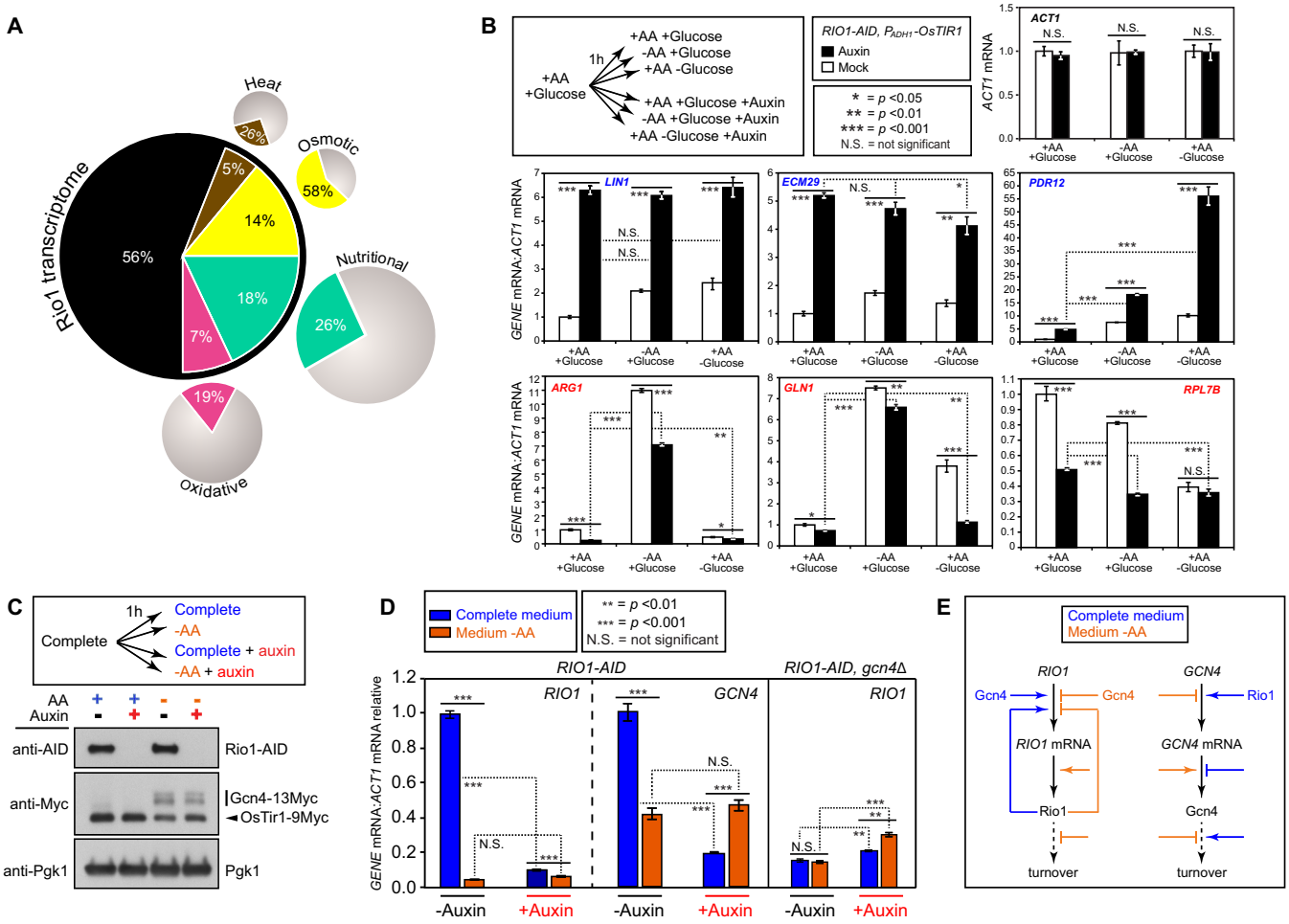

Figure 7. Rio1 responds to nutritional deprivation and crosstalks with Gcn4 at the transcriptional level. (**A**) The Rio1 transcriptome is enriched in transcripts of genes that are part of various stress-response systems. The main pie shows the percentage of the 818 Rio1-modulated genes that belong to specific stress transcriptomes (represented by the peripheral pies, which are size-weighted for the number of genes they contain (listed in Supplementary Table S10). The slices indicate the % of overlap at the gene level between the Rio1 and stress-response transcriptomes. *P*-values quantitating the significance of these overlaps (determined with Fischer's exact test) are listed in the text. (**B**) Expression analysis of 6 Rio1-regulated reporter genes in yeast growing in complete synthetic medium (+amino acids [AA] +2% glucose) or in synthetic medium lacking AA or glucose. Blue: gene whose transcript levels decrease due to Rio1 activity. Red: gene whose transcript levels increase due to Rio1 activity. White bars: Rio1-containing cells, black bars: Rio1-depleted cells. Transcript concentrations were measured by TaqMan-based RT-qPCR analysis and normalized to those of *ACT1* (encoding actin, *ACT1* mRNA levels are plotted in the upper right graph). Numbers were then correlated to those calculated for the mock-treated cells grown in complete synthetic medium. Error bars = standard errors. The RT-qPCR data are listed in Supplementary Table S11. The levels of confidence (*P*-values) that the differences between the indicated datasets are (non)significant are symbolically represented by stars, and were calculated with the unpaired, two-tailed student *t*-test. The levels of confidence of the differences that exist between the data measured in the mock-treated cultures (*P*-values) are indicated in Supplementary Figure S12. (**C**) Experimental outline and western hybridization blots evidencing the levels of Rio1-AID, Gcn4-13Myc and OsTir1-9Myc (anti-Myc) in the *RIO1-AID, P_{ADH1}-OsTIR1-9Myc, GCN4-13Myc* strain that was grown exponentially in complete 2% glucose synthetic medium, and then shifted for 1 h to complete 2% glucose synthetic medium containing or lacking AA, that was further provided with 500 μm of auxin or mock solution. 3-Phosphoglycerate kinase Pgk1 acted as the loading control (as did the exogenous auxin receptor OsTir1-9Myc). (**D**) *RIO1* and *GCN4* mRNA levels measured by TaqMan-based RT-qPCR analysis in *RIO1-AID, P_{ADH1}-OsTIR1-9Myc* (named *RIO1-AID*) and *RIO1-AID, P_{ADH1}-OsTIR1-9Myc, gcn4Δ* (named *RIO1-AID, gcn4Δ*) cells grown in complete, 2% glucose synthetic medium, followed by a 1 h shift to complete, 2% glucose medium (blue bar, black underline), 2% glucose medium lacking AA (orange bar, black underline), complete 2% glucose medium provided with 500 μm of auxin (blue bar, red underline) or 2% glucose medium lacking AA but containing 500 μm of auxin (orange bar, red underline). *RIO1* and *GCN4* transcript levels were normalized to those of *ACT1* and then to their respective values measured in the cells grown in complete 2% glucose medium lacking auxin (value = 1). Error bars = standard errors. The levels of confidence (*P*-values) are indicated by stars and were calculated with the unpaired, two-tailed student *t*-test (**E**) Graphic summary of the data shown in panels (C) and (D).

we found that the connection between the oxidative stress regulon and that of Rio1 became non-significant (Fisher's exact test; *P*-value = 0.09). This finding indicated that the overlap between both regulons is due to their shared control of ribosome biology. The overlaps between Rio1 and the heat, osmotic, and nutritional regulons remained highly significant (*P*-values = 1.7E-11, 3.2E-23 and 2.9E-12, respectively), indicating a shared response to extracellular cues that covers but also extends way beyond regulating ribosome production and activity.

Since the Rio1 transcriptome shares 18% of its genes with nutritional stress regulons (Figure 7A), we decided to examine the response of Rio1 to sugar and amino acid availability. Specifically, we chose six Rio1 target genes as response readouts that represent various cell biological activities (Supplementary Table S5 and Figure S5D). They include the Rio1 downregulated *LIN1* (encodes a U5 snRNP protein that is also involved in regulating cohesin), *ECM29* (encodes a protein that assists in the association of the core and regulatory particles of the 26S proteasome) and *PDR12* (encodes a plasma membrane ATP-binding cassette transporter), next to the Rio1 upregulated *GLN1* (encodes L-glutamine synthetase 1, which synthesizes L-glutamine from L-glutamate and ammonia), *RPL7B* (encodes 60S ribosomal subunit protein L7B) and *ARG1* (encodes argininosuccinate synthetase 1, which catalyzes the formation of L-argininosuccinate from L-citrulline and L-aspartate). Three *RIO1-AID* yeast cultures were grown exponentially in complete 2% glucose synthetic medium. Each culture was then split in six. The cells were washed and transferred to synthetic medium lacking amino acids or glucose and were supplemented with 500 μM of auxin or a mock solution (graphically summarized in Figure 7B). After 1 h, the cells were isolated and the transcripts of our reporter genes quantitated by TaqMan RT-qPCR analysis (the measured data are tabulated in Supplementary Table S11). Since *ACT1* transcript levels did not change in response to the short nutritional shift, we used them as the internal reference (upper right plot, Figure 7B). In the mock-treated cells (white bars) shifted from complete medium to medium lacking amino acids or glucose; our reporter genes responded in significant fashion to at least one condition of nutritional depletion (Figure 7B, *P*-values are indicated in Supplementary Figure S12). In the absence of Rio1 activity (black bars), the reporter genes responded significantly: the transcript levels of *LIN1*, *EMC29* and *PDR12* strongly increased (derepressed and/or stabilized) whereas those of *ARG1*, *GLN1* and *RPL7B* significantly dropped in at least one condition of nutritional deprivation (*P*-values for the shifts are indicated in Figure 7B). These observations strongly indicate that Rio1 regulates its network, and hence yeast biology, in response to the nutritional resources that are available.

Rio1 and Gcn4 crosstalk in response to amino acid starvation

After confirming that Rio1 responds to nutrient availability, we decided to expand upon this finding. We also wished to experimentally validate our computed network and probe the regulation of Rio1 upon starvation. The ResponseNet algorithm indicated that Rio1 employs a series of transcription factors, including Gcn4, to manage its gene targets (Supplementary Figure S10). Gcn4 is a key determinant of the cellular adaptation to amino acid deprivation (112). To experimentally validate our network, we focused on nitrogen depletion and assessed the impact of Gcn4 on the amino acid response as mediated by Rio1. Reversely, we probed the contribution of Rio1 to Gcn4 activity. Specifically; *RIO1-AID GCN4-13Myc* cells were grown exponentially in complete 2% glucose synthetic medium. The culture was then split in four, the cells washed and transferred for 1h to 2% glucose synthetic medium containing or lacking amino acids, and provided with 500 μM of auxin or a mock solution (graphically summarized in Figure 7C). The experiments were performed in triplicate. While the shift from complete medium to mock-treated amino acid-deprived medium did not affect Rio1 protein levels (lane 1 versus lane 3 in anti-AID western blot, Figure 7C), the number of its transcripts fell dramatically (blue bar -auxin versus orange bar -auxin; Figure 7D), suggesting that *RIO1* mRNA translation and/or Rio1 protein stability increased during amino acid starvation. Depleting Rio1 during amino acid deprivation (confirmed by the absence of Rio1-AID signals in the western blot; lane 2 versus lane 4) lead to a decrease in *RIO1* transcript levels (blue bar +auxin versus orange bar +auxin), implying transcriptional auto-repression or increased *RIO1* transcript turnover under nutritional stress conditions. Depleting Rio1 in complete medium strongly reduced *RIO1* transcript levels (blue bar −auxin versus blue bar +auxin), implying transcriptional auto-activation or increased *RIO1* transcript stability under nutritionally rich conditions (all RT-qPCR data are tabulated in Supplementary Table S12). While Rio1 was shown to activate itself *in vitro* by auto-phosphorylation (2,16,69) our findings suggest auto-regulation also at the transcriptional level in cells. We note that our ChIP-Seq experiments did not identify a Rio1 footprint in the *RIO1* promoter sequence. As such, Rio1 may regulate its own transcription off-DNA or act with high kinetics, preventing us from capturing the interaction with its own promoter.

In yeast grown in complete medium we did not detect the Gcn4 protein (lane 1 in anti-Myc western blot, Figure 7C), as expected, due to its high turnover in rich conditions (half-life ∼2 min (113–115). The same was true for cells grown in complete medium and depleted of Rio1 (lane 2 in anti-Myc western blot). In both cases, we nevertheless detected *GCN4* transcripts (but *GCN4* transcript levels were 80% lower in the cells depleted of Rio1) (blue bar −auxin versus blue bar +auxin). This finding suggests that despite the active turnover of Gcn4, Rio1 upregulates *GCN4* expression and/or stabilizes the *GCN4* transcripts in yeast grown in complete medium, confirming our RNA-Seq results. Taken together, we corroborate that in rich medium *GCN4* mRNA translation diminishes (113) and that Gcn4 becomes actively turned over (114,115). Upon amino acid deprivation, the Gcn4 protein accumulated (lane 1 versus lane 3 in anti-Myc western blot) while *GCN4* transcript levels dropped with 60% (blue bar -auxin versus orange bar −auxin). Shifting the cells from complete to amino acid-depleted medium in the absence of Rio1 did not further affect Gcn4 protein levels (lane 2 versus lane 4). However, the latter nutritional downshift led to an increase in *GCN4* transcript levels (blue bar +auxin versus orange bar +auxin),

indicating reduced *GCN4* mRNA translation and/or improved Gcn4 stability (half-life ∼10 min (114)).

To examine whether Gcn4 affects *RIO1* expression, as suggested by Rio1's network (Supplementary Figure S10), we grew *RIO1-AID,* and *RIO1-AID gnc4Δ* strains exponentially in complete synthetic 2% glucose medium. The cultures were then split in four, the cells washed and transferred for 1 h to 2% glucose medium containing or lacking amino acids, and provided with 500 μM of auxin or with a mock solution. The experiments were performed in triplicate. RT-qPCR analyses revealed that Gcn4 activates *RIO1* expression in complete medium (first blue bar −auxin versus third blue bar −auxin) while Gcn4 represses *RIO1* in medium lacking amino acids (blue bar +auxin versus orange bar +auxin and orange bar −auxin versus orange bar +auxin), reinforcing their cross-regulatory relationship (all above observations are summarized in Figure 7E).

To determine whether Rio1 and Gcn4 also independently modulate the target genes they share (Supplementary Table S9), we measured in the *RIO1-AID* and *RIO1-AID gnc4Δ* strains the transcription of 10 reporter genes under the above nitrogen downshift conditions (the RT-qPCR data are tabulated in Supplementary Table S12 and are plotted in Supplementary Figure S13A). It is well-known (116) that during amino acid starvation, Gcn4 activates *ARG5,6*, *ASN1*, *ILV5*, *MET6*, *SER3*, *BNT2*, *SNZ1* and *SUL2*, and in parallel represses *RPLB7* and *GLN1*. In rich medium, Rio1 activates *ARG5,6*, *ASN1*, *GLN1*, *ILV5*, *MET6, SER3* and *RPLB7,* represses *BTN2,* but does not affect *SNZ1* and *SUL2* (Supplementary Table S5). *RIO1* and *GCN4* were probed as internal controls. In short, our starvation experiments confirmed the reported transcriptional control by Gcn4 of its target genes under rich and amino acid-depleted conditions (116). However, we now add the involvement of Rio1 to this regulation since Rio1 activity either strengthened or opposed the housekeeping effect of Gcn4 on its gene targets. Reversely, the same is true for Gcn4, which similarly modulates the Rio1 gene targets (graphically summarized in Supplementary Figure S13B).

Taken together, the above experiments verified Rio1's response network as we confirmed an intricate interplay between Rio1 and transcription factor Gcn4. Both cross-regulate each other at the transcriptional level and fine-tune the expression of their shared target genes to ensure a swift, global response to nutritional stress.

Establishing the RIOK1 interactome

The contributions of Rio1 to pre-rRNA processing and small ribosomal subunit maturation have been confirmed for RIOK1 in human cells (8,10,15). As such, we asked whether RIOK1 similarly engages in the spectrum of activities revealed here for Rio1. To answer this question, we scanned the literature, public and commercial repositories for RIOK1 interactors and recovered 352 proteins from 14 proteomic studies (Supplementary Table S13). By weighing and functionally clustering these interactors, we generated the RIOK1–protein interaction map (Figure 8; enrichment *P*-values are listed in the figure legend). It comprises the same core activity groups (GO classifications) as the yeast Rio1 interactome (Figure 1A), strongly arguing for an evolutionary conservation of Rio1 and RIOK1 biologies.

DISCUSSION

To survive and reproduce in a constantly changing environment, yeast must quickly assess and transmit the nature and levels of available nutrients into its metabolic, growth and cell division programs. To maximize fitness under the conditions sensed, yeast has evolved signaling networks including those centered around the Ras/protein kinase A, the AMP-activated kinase and the TORC kinase complexes, that guide transcriptional, translational, post-translational, metabolic and developmental decisions (18). The presence of nutrients determines proliferation, a resource and energy-demanding process that primarily depends on the cell's biosynthetic capacity, provided by ribosomes (117). Our present study has identified Rio1 as the upstream regulator of a new, essential and conserved nutrient-response network. Rio1 governs its network by involving a host of regulators and intermediate factors that it modulates either directly or indirectly at the protein, RNA and/or gene levels. Whether Rio1 acts upon its network members (proteins, ORFs, RNAs) and pathways as a kinase and/or ATPase remains to be determined. The purpose of Rio1 and its network is to promote growth and division when conditions are favorable, and to restrain them during nutrient deprivation. In this respect, the Rio1 network is functionally analogous to that managed by the conserved Tor1 kinase complex (TORC1). Indeed, the Tor1 kinase regulates at the protein and gene levels *35S* rDNA transcription, pre-rRNA processing, ribosome protein expression and assembly, mRNA processing, protein stability, nutrient transport and autophagy (118). The Tor1 and Rio1 networks share 68 target genes (Tor1 regulates an additional 398 genes (119)). However, this overlap is not statistically significant (Fisher's exact test, *P*-value = 6.4E-02). Since Rio1 and the Tor1 kinase complex do not physically interact, and since Rio1 does not affect *TOR1* expression (and *vice versa*), both kinase networks sustain the nutrient response in parallel fashion.

While we demonstrated that carbon and nitrogen levels are upstream cues, comparative analyses suggested that Rio1 and its network may manage additional stresses (Figure 7A). In that respect, it may be more broad-acting than the TORC1 network. While Rio1 and Tor1 act in parallel, the Rio1 network is closely integrated with other response networks driven by additional kinases (Figure 1B) and key transcription factors. The latter include the networks managed by Gcn4 [67 genes shared with Rio1, 195 additional], Rpn4 [62, 92] and Rap1 [104, 99] (Fisher's exact test *P*-values = 1.2E-09, 4.1E-19 and 2.3E-43, respectively) (18,117,120,121) (Supplementary Figure S13 and Table S9).

From the Rio1–protein interaction map, its regulon and genetic diagrams, it is evident that Rio1 controls growth foremost by influencing protein synthesis and turnover. Indeed, of its 818 gene/transcript targets, 226 are dedicated to ribosome production and translation activity, while an additional 97 are involved in protein folding and degradation (a combined 323 genes = 39% of the Rio1 regulon). Simi-

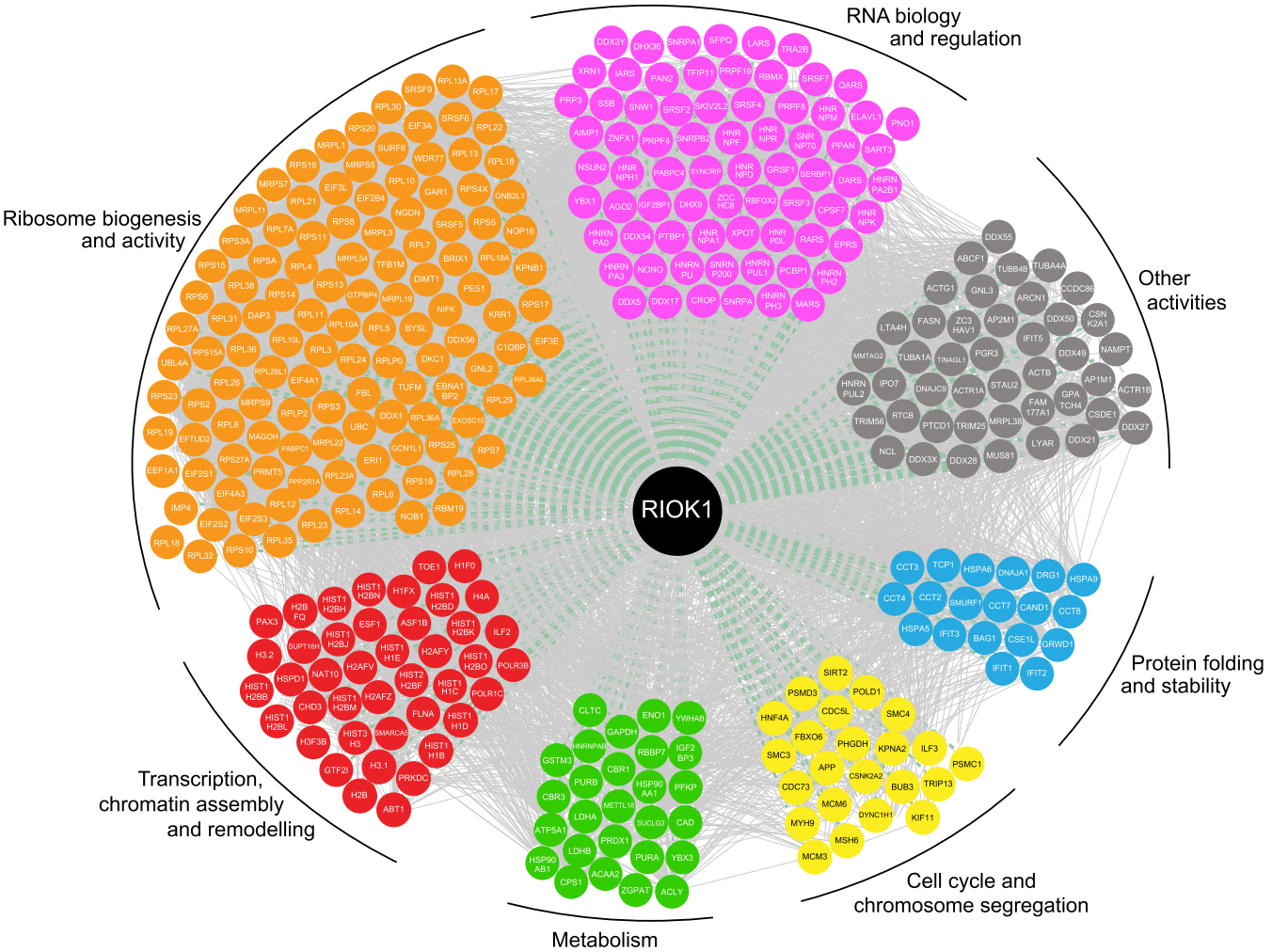

Figure 8. The human RIOK1–protein interaction map. The interaction network comprises 352 proteins that were identified in co-purifications reported in 14 publications (Supplementary Table S13). RIOK1 and its partners are connected by green lines while protein interactions between the RIOK1 interactors themselves are shown by gray lines in the background. The RIOK1 interactors were functionally clustered using the Gene Ontology term 'Biological Process' that is associated with each protein. The *P*-values of the functional enrichments are: ribosome biogenesis and activity = 4.2E-25, RNA biology and regulation = 2.4E-54, protein folding and stability = 8.6E-03, cell cycle and chromosome segregation = 1.3E-02, metabolism = 5.8E-21, transcription, chromatin assembly and remodeling = 1.7E-23.

larly, Rio1 physically interacts with 35 proteins involved in ribosome biogenesis, activity and protein governance.

Typical Ribi gene products help ribosomes become operational protein-synthesis machines (pre-rRNA processing, folding, nuclear export of pre-ribosomal particles to the cytoplasm, maturation and assembly events, etc.). As demonstrated previously, Rio1 serves the Ribi program by regulating *35S* rDNA transcription, pre-rRNA processing and 40S ribosomal subunit maturation. However, we find that Rio1 also contributes by regulating the expression of 20% of the Ribi regulon members, including ORFs that encode components of the small subunit processome (122,123)) and proteins that mediate ribosome assembly, maturation, export, translation initiation and termination (Supplementary Table S5). Rio1 also physically interacts with proteins contributing to ribosome biogenesis and mRNA translation in events beyond those associated with Rio1 activity today. Since Rio1 strongly genetically interacts with the Dom34:Hbs1 complex (94), which dissolves stalled ribosomes (124), and also physically interacts with Zuo1, a ribosome-associated chaperone for nascent polypeptide chains (91), Rio1 could well be involved in surveying the quality of ribosomes and the proteins they deliver. Being a Ribi member, we for sure did not expect Rio1 to transcriptionally regulate the RP regulon, encoding the structural RPs. Their promoters share binding sites for RP-specific transcriptional activators, including Rap1, which we identified as a Rio1 gene target. Hence, Rio1 may command ribosome expression in part directly (footprints identified in promoters of ORFs encoding RPs, Figure 4A) and by regulating *RAP1* transcription and/or *RAP1* mRNA stability (Supplementary Figure S11B).

Nitrogen availability not only decides on ribosome production and protein synthesis, but also on protein turnover (restrained under rich conditions, active during amino acid deprivation). Consistent with this, we find that Rio1 down-

regulates the expression of all subunits of the 26S proteasome under nitrogen-rich conditions. This likely occurs via Rpn4, the transcription factor for all proteasomal proteins, which we identified as a Rio1 gene target (Supplementary Figure S11A). Besides determining its expression, Rio1 may also promote proteasome formation as it regulates the expression of 26S proteasomal assembly factor Rpn6. Furthermore, Rio1 and its network manage the transcription of enzymes constituting the ubiquitin pathway. Its localization to vacuoles (peptidase- and proteinase-catalyzed protein turnover compartments), physical interaction with and control of genes involved in autophagy and cytosol-to-vacuole pathways are in line with Rio1 supervising protein governance at a global scale. Fittingly, Rio1 physically interacts with and regulates the expression of numerous chaperones.

Ribosome production, mRNA translation and cell growth are highly demanding from a substrate and energy point of view. Also, available nutrients need to be uptaken and transported internally. Hence, it is not surprising that part of Rio1's network (11 protein interactors, 306 gene targets = 37% of its regulon) is dedicated to metabolism (nutrient uptake and transport, carbohydrate, amino acid, lipid, purines, pyrimidines and vitamins) and energy production (glycolysis, mitochondrial respiration, ATP synthase–ATPase complex subunits), as is its localization to the mitochondria. Importantly, the majority of these genes (83%) are upregulated together with ribosome production and protein synthesis under rich conditions.

While Rio1 stimulates growth and survival, its also promotes physiology (protein movement, transport) and cell division. Rio1 was already shown to ensure a timely entry into the cell cycle by regulating directly RNA polymerase I activity at the rDNA array. In addition, repressing rDNA transcription allows for rDNA condensation, which finalizes the chromosome segregation process in late anaphase (16). During DNA replication, repression of rDNA transcription by Rio1 also reduces local collisions between RNA polymerase I and the replisome. This minimizes rDNA double strand breaks, hyper-recombinations within and between sister rDNA arrays, resulting in a loss of or increase in rDNA units. Importantly, ribosome biosynthetic activity is linked to the rDNA gene copy number within the rDNA array (125,126). As such, one might hypothesize that the transcriptional regulation of RNA polymerase I by Rio1 could lead to a controlled increase or decrease in rDNA repeats to enhance or reduce ribosome production capacity depending on nutritional resources. We have experimentally confirmed that Rio1 acts positively toward replication fork stability/progression at the rDNA (Figure 2B and C). Since Rio1 physically and functionally interacts with various proteins mediating DNA repair and recombination, the role of its network in ensuring genetic stability during cell division is likely more multifaceted than currently appreciated. Its localization to kinetochores (physically interacts with conserved subunit Mcm21^{CENP-O}) implies an important role in chromosome transmission and may explain the increased level of aneuploidy, measured in yeast suffering from reduced Rio1 activity (88).

Telomere-length homeostasis depends on a large genetic network that is regulated in part by Rio1 gene-target *RAP1* (127). This network is disrupted by environmental stress signals, resulting in altered telomere length and adverse effects on lifespan. While Rio1 regulates *RAP1* expression, other Rio1 target genes (including *DAP1*, *HTL1*, *OPI1*, *SDC1*, *STM1* and *XRN1*) are involved in telomere maintenance and silencing. In addition, Rio1 physically interacts with the DNA helicase Y'-Help1 (128) and the conserved protein Elg1 (129), which protect telomere length and stability, suggesting that the Rio1 contributes to telomere stability and timely ageing.

During our study, we also probed the regulation of *RIO1* expression and found it to be auto-regulated and sustained by nutrient-stress transcription factor Gcn4, which determines the expression of amino acid biosynthetic genes. Similarly, Rio1 modulates *GCN4* expression, revealing cross-regulation, as was suggested by our algorithm that assembled the Rio1 network (Supplementary Figure S10). This observation is especially striking since control of Gcn4 activity was considered to occur only at the level of *GCN4* transcript translation and Gcn4 stability and turnover (112,130). Rio1 could regulate *GCN4* expression via transcription factors Hap4 and Fkh2 (Y2H interactors of Rio1), which localize to the *GCN4* promoter (131,132). In turn, the Gcn4 consensus binding sequence 5′-TGACTC-3′ (133–135) lies 90 bp upstream of *RIO1*'s transcription initiation site. Furthermore, while *RIO1* expression is reduced under nutritionally poor conditions, Rio1 protein stability increases. The same is true for Gcn4. Future inquiries into the Rio1-Gcn4 axis promise to significantly advance our understanding of the nitrogen starvation response in yeast and species beyond.

Rio1 protein numbers (536 molecules/cell (136)) are in line with those measured for other network kinases, including Tor1 (225–589 molecules/cell (136,137)). By interacting with a portfolio of regulators, kinases, phosphatases, transcription factors, etc. Rio1—similar to other network kinases—can amplify its activity to manage its network.

For most nutrient signaling pathways, the signal receptors and transduction processes are barely understood (138). When amino acid levels increase in the lysosome (the proteins(s) sensing this change are unknown), human mTORC1 is activated by recruitment to the lysosome surface (equivalent of the yeast vacuole) (139). The AMP-activated protein kinase responds to increased AMP:ATP ratios as a surrogate for glucose abundance (140). Could Rio1 similarly sense and transduce energy levels into its network as it may also act as an ATPase (so far reported only for pre-40S ribosomal subunit maturation) (8,9) and since Rio1 localizes to the ATP-generating mitochondria? Does Rio1 signaling depend on other sensor kinases (including Ck2, Sch9, Psk1 and Rim15) or protein phosphatases (including Pho8, Pah1, Cdc14, Psy2 and Yvh1) with which it physically or genetically interacts? Answering these questions represent important challenges for the future.

We believe that our singular datasets and integrated network (analyzable and manipulatable at http://netbio.bgu.ac.il/respnet/ by adding the Rio1 protein and gene targets) represent valuable resources that will advance the understanding of biological processes now associated with Rio1 activity. For example, yeast depleted of Rio1 displays a chain-like morphology after two to three cell cycles (Supplementary Figure S3G). We found that Rio1 physically in-

teracts with septin ring component Cdc12 and with the morphogenesis checkpoint kinase Hsl1, which are required for cytokinesis (141) and for coupling bud formation to cell cycle progression (142), respectively. A lack of Rio1-based regulation of both proteins could explain the chain-like phenotype of the Rio1-AID depleted strain, typical of a cytokinesis defect. The covert sensitivity of heterozygous *rio1Δ* yeast to drugs interfering with sphingolipid and ergosterol synthesis (20) is coherent with our finding that Rio1 controls the transcription of genes catalyzing sphingolipid and ergosterol synthesis (Supplementary Table S5).

In human cells, *RIOK1* expression is activated by the proto-oncogenic transcription factor c-Myc (143) whose amplification in ∼20% of all cancers correlates with metastasis and poor prognosis (144). In turn, RIOK1—as part of the PRMT5 complex—promotes the translation of c-Myc transcripts (26). Hence, it is not surprising that *RIOK1* is overexpressed in myriad malignancies (145). c-Myc activates genes involved in ribosome biogenesis, mitochondrial activity (respiration, glycolytic flux), metabolism, nucleotide and lipid synthesis, and cell-cycle progression; thereby enhancing the ability of a cancer cell to transform, grow and proliferate (144,146). Since the cellular processes controlled by c-Myc significantly overlap with those identified here for Rio1 (and RIOK1), overexpression of RIOK1 by c-Myc could be an important contributor to the transformation capacity of c-Myc.

DATA AVAILABILITY

The RNA-Seq and ChIP-Seq data are available at GSE70287 (GEO).

SUPPLEMENTARY DATA

Supplementary Data are available at NAR Online.

ACKNOWLEDGEMENTS

We thank Jolanda van Leeuwen for communicating the mutations in the *rio1-5001* allele.
Authors' contribution: M.G.I. performed most of the biological experiments. M.B. analyzed the protein-interaction, genetic-interaction and gene-expression datasets to produce the weighted interactome and transcriptome maps. O.B. and E.Y.-L. performed the ResponseNet analyses. L.G. and W.C. analyzed the RNA-Seq and ChIP-Seq data, respectively. C.G. and M.D.M. performed the genetic interaction studies. V.I. did the ChIP-chip experiment, while C.V. and R.V. localized Rio1-GFP via indirect IF imaging. G.V.B. and A.A.M. localized Rio1-GFP via indirect cryo-immunogold EM. B.S., C.R.J. and D.B. examined the contribution of Rio1 to rDNA and ARS305 replication. S. F.-C. profiled ribosomes and examined the neo-synthesis of RNAs and proteins in the presence and absence of Rio1 activity. M.G.I. and P.D.W. conceived and interpreted the experiments, and wrote the paper. All authors have approved the manuscript.

FUNDING

Howard Hughes Medical Institute International Early Career Scientist Grant and Italian Association for Cancer Research (A.I.R.C.) Investigator Grant 16886 to R.V.; European Research Council Consolidator Grant 682190 and A.I.R.C. Investigator Grant 18976 to D.B.; Intramural Funds from the Department of Biochemistry III "House of the Ribosome" and DFG Collaborative Research Centre Grant SFB960-AP1 to S.F.-C.; United States-Israel Binational Science Foundation Grant 2011296 to E.Y.-L.; A.I.R.C. Investigator Grant 13243 to P.D.W.. Funding for open access charge: A.I.R.C. Investigator Grant 13243 to P.D.W..
Conflict of interest statement. None declared.

REFERENCES

1. Esser,D. and Siebers,B. (2013) Atypical protein kinases of the RIO family in archaea. *Biochem. Soc. Trans.*, **41**, 399–404.
2. Laronde-Leblanc,N., Guszczynski,T., Copeland,T. and Wlodawer,A. (2005) Structure and activity of the atypical serine kinase Rio1. *FEBS J.*, **272**, 3698–3713.
3. LaRonde-LeBlanc,N. and Wlodawer,A. (2005) A family portrait of the RIO kinases. *J. Biol. Chem.*, **280**, 37297–37300.
4. LaRonde-LeBlanc,N. and Wlodawer,A. (2005) The RIO kinases: an atypical protein kinase family required for ribosome biogenesis and cell cycle progression. *Biochim. Biophys. Acta*, **1754**, 14–24.
5. LaRonde,N.A. (2014) The ancient microbial RIO kinases. *J. Biol. Chem.*, **289**, 9488–9492.
6. Knuppel,R., Christensen,R.H., Gray,F.C., Esser,D., Strauss,D., Medenbach,J., Siebers,B., MacNeill,S.A., LaRonde,N. and Ferreira-Cerca,S. (2018) Insights into the evolutionary conserved regulation of Rio ATPase activity. *Nucleic Acids Res.*, **46**, 1441–1456.
7. Ferreira-Cerca,S., Sagar,V., Schafer,T., Diop,M., Wesseling,A.M., Lu,H., Chai,E., Hurt,E. and LaRonde-LeBlanc,N. (2012) ATPase-dependent role of the atypical kinase Rio2 on the evolving pre-40S ribosomal subunit. *Nat. Struct. Mol. Biol.*, **19**, 1316–1323.
8. Ferreira-Cerca,S., Kiburu,I., Thomson,E., LaRonde,N. and Hurt,E. (2014) Dominant Rio1 kinase/ATPase catalytic mutant induces trapping of late pre-40S biogenesis factors in 80S-like ribosomes. *Nucleic Acids Res.*, **42**, 8635–8647.
9. Turowski,T.W., Lebaron,S., Zhang,E., Peil,L., Dudnakova,T., Petfalski,E., Granneman,S., Rappsilber,J. and Tollervey,D. (2014) Rio1 mediates ATP-dependent final maturation of 40S ribosomal subunits. *Nucleic Acids Res.*, **42**, 12189–12199.
10. Baumas,K., Soudet,J., Caizergues-Ferrer,M., Faubladier,M., Henry,Y. and Mougin,A. (2012) Human RioK3 is a novel component of cytoplasmic pre-40S pre-ribosomal particles. *RNA Biol.*, **9**, 162–174.
11. Belhabich-Baumas,K., Joret,C., Jady,B.E., Plisson-Chastang,C., Shayan,R., Klopp,C., Henras,A.K., Henry,Y. and Mougin,A. (2017) The Rio1p ATPase hinders premature entry into translation of late pre-40S pre-ribosomal particles. *Nucleic Acids Res.*, **45**, 10824–10836.
12. Vanrobays,E., Gleizes,P.E., Bousquet-Antonelli,C., Noaillac-Depeyre,J., Caizergues-Ferrer,M. and Gelugne,J.P. (2001) Processing of 20S pre-rRNA to 18S ribosomal RNA in yeast requires Rrp10p, an essential non-ribosomal cytoplasmic protein. *EMBO J.*, **20**, 4204–4213.
13. Vanrobays,E., Gelugne,J.P., Gleizes,P.E. and Caizergues-Ferrer,M. (2003) Late cytoplasmic maturation of the small ribosomal subunit requires RIO proteins in Saccharomyces cerevisiae. *Mol. Cell. Biol.*, **23**, 2083–2095.
14. Hector,R.D., Burlacu,E., Aitken,S., Bihan,T.L., Tuijtel,M., Zaplatina,A., Cook,A.G. and Granneman,S. (2014) Snapshots of pre-rRNA structural flexibility reveal eukaryotic 40S assembly dynamics at nucleotide resolution. *Nucleic Acids Res.*, **42**, 12138–12154.
15. Widmann,B., Wandrey,F., Badertscher,L., Wyler,E., Pfannstiel,J., Zemp,I. and Kutay,U. (2012) The kinase activity of human Rio1 is required for final steps of cytoplasmic maturation of 40S subunits. *Mol. Biol. Cell*, **23**, 22–35.

16. Iacovella,M.G., Golfieri,C., Massari,L.F., Busnelli,S., Pagliuca,C., Dal Maschio,M., Infantino,V., Visintin,R., Mechtler,K., Ferreira-Cerca,S. *et al.* (2015) Rio1 promotes rDNA stability and downregulates RNA polymerase I to ensure rDNA segregation. *Nat. Commun.*, **6**, 6643.
17. Bosio,M.C., Fermi,B. and Dieci,G. (2017) Transcriptional control of yeast ribosome biogenesis: a multifaceted role for general regulatory factors. *Transcription*, **8**, 254–260.
18. Broach,J.R. (2012) Nutritional control of growth and development in yeast. *Genetics*, **192**, 73–105.
19. Wade,C.H., Umbarger,M.A. and McAlear,M.A. (2006) The budding yeast rRNA and ribosome biosynthesis (RRB) regulon contains over 200 genes. *Yeast*, **23**, 293–306.
20. Lee,A.Y., St Onge,R.P., Proctor,M.J., Wallace,I.M., Nile,A.H., Spagnuolo,P.A., Jitkova,Y., Gronda,M., Wu,Y., Kim,M.K. *et al.* (2014) Mapping the cellular response to small molecules using chemogenomic fitness signatures. *Science*, **344**, 208–211.
21. Durut,N. and Saez-Vasquez,J. (2015) Nucleolin: dual roles in rDNA chromatin transcription. *Gene*, **556**, 7–12.
22. Tajrishi,M.M., Tuteja,R. and Tuteja,N. (2011) Nucleolin: the most abundant multifunctional phosphoprotein of nucleolus. *Commun. Itegr. Biol.*, **4**, 267–275.
23. Guderian,G., Peter,C., Wiesner,J., Sickmann,A., Schulze-Osthoff,K., Fischer,U. and Grimmler,M. (2011) RioK1, a new interactor of protein arginine methyltransferase 5 (PRMT5), competes with pICln for binding and modulates PRMT5 complex composition and substrate specificity. *J. Biol. Chem.*, **286**, 1976–1986.
24. Read,R.D., Fenton,T.R., Gomez,G.G., Wykosky,J., Vandenberg,S.R., Babic,I., Iwanami,A., Yang,H., Cavenee,W.K., Mischel,P.S. *et al.* (2013) A kinome-wide RNAi screen in Drosophila Glia reveals that the RIO kinases mediate cell proliferation and survival through TORC2-Akt signaling in glioblastoma. *PLos Genet.*, **9**, e1003253.
25. Zhao,Q., Rank,G., Tan,Y.T., Li,H., Moritz,R.L., Simpson,R.J., Cerruti,L., Curtis,D.J., Patel,D.J., Allis,C.D. *et al.* (2009) PRMT5-mediated methylation of histone H4R3 recruits DNMT3A, coupling histone and DNA methylation in gene silencing. *Nat. Struct. Mol. Biol.*, **16**, 304–311.
26. Gao,G., Dhar,S. and Bedford,M.T. (2017) PRMT5 regulates IRES-dependent translation via methylation of hnRNP A1. *Nucleic Acids Res.*, **45**, 4359–4369.
27. Luo,J., Emanuele,M.J., Li,D., Creighton,C.J., Schlabach,M.R., Westbrook,T.F., Wong,K.K. and Elledge,S.J. (2009) A genome-wide RNAi screen identifies multiple synthetic lethal interactions with the Ras oncogene. *Cell*, **137**, 835–848.
28. Cox,A.D. and Der,C.J. (2010) Ras history: the saga continues. *Small GTPases*, **1**, 2–27.
29. Goitre,L., Trapani,E., Trabalzini,L. and Retta,S.F. (2014) The Ras superfamily of small GTPases: the unlocked secrets. *Methods Mol. Biol.*, **1120**, 1–18.
30. Weinberg,F., Reischmann,N., Fauth,L., Taromi,S., Mastroianni,J., Kohler,M., Halbach,S., Becker,A.C., Deng,N., Schmitz,T. *et al.* (2017) The atypical kinase RIOK1 promotes tumor growth and invasive behavior. *EBioMedicine*, **20**, 79–97.
31. Kiburu,I.N. and LaRonde-LeBlanc,N. (2012) Interaction of Rio1 kinase with toyocamycin reveals a conformational switch that controls oligomeric state and catalytic activity. *PLoS One*, **7**, e37371.
32. Kubinski,K., Maslyk,M. and Orzeszko,A. (2017) Benzimidazole inhibitors of protein kinase CK2 potently inhibit the activity of atypical protein kinase Rio1. *Mol. Cell. Biochem.*, **426**, 195–203.
33. Mielecki,M., Krawiec,K., Kiburu,I., Grzelak,K., Zagorski,W., Kierdaszuk,B., Kowa,K., Fokt,I., Szymanski,S., Swierk,P. *et al.* (2013) Development of novel molecular probes of the Rio1 atypical protein kinase. *Biochim. Biophys. Acta*, **1834**, 1292–1301.
34. Nishimura,K., Fukagawa,T., Takisawa,H., Kakimoto,T. and Kanemaki,M. (2009) An auxin-based degron system for the rapid depletion of proteins in nonplant cells. *Nat. Methods*, **6**, 917–922.
35. Rain,J.C., Selig,L., De Reuse,H., Battaglia,V., Reverdy,C., Simon,S., Lenzen,G., Petel,F., Wojcik,J., Schachter,V. *et al.* (2001) The protein-protein interaction map of Helicobacter pylori. *Nature*, **409**, 211–215.
36. Wojcik,J., Boneca,I.G. and Legrain,P. (2002) Prediction, assessment and validation of protein interaction maps in bacteria. *J. Mol. Biol.*, **323**, 763–770.
37. Fromont-Racine,M., Rain,J.C. and Legrain,P. (1997) Toward a functional analysis of the yeast genome through exhaustive two-hybrid screens. *Nat. Genet.*, **16**, 277–282.
38. Formstecher,E., Aresta,S., Collura,V., Hamburger,A., Meil,A., Trehin,A., Reverdy,C., Betin,V., Maire,S., Brun,C. *et al.* (2005) Protein interaction mapping: a Drosophila case study. *Genome Res.*, **15**, 376–384.
39. Beznoussenko,G.V., Ragnini-Wilson,A., Wilson,C. and Mironov,A.A. (2016) Three-dimensional and immune electron microscopic analysis of the secretory pathway in Saccharomyces cerevisiae. *Histochem. Cell Biol.*, **146**, 515–527.
40. Mironov,A.A. Jr and Mironov,A.A. (1998) Estimation of subcellular organelle volume from ultrathin sections through centrioles with a discretized version of the vertical rotator. *J. Microsc.*, **192**, 29–36.
41. Griffiths,G. (1993) *Fine Structure Immunocy to chemistry*. Springer-Verlag, Berlin, Heidelberg, p. 459.
42. Fumasoni,M., Zwicky,K., Vanoli,F., Lopes,M. and Branzei,D. (2015) Error-free DNA damage tolerance and sister chromatid proximity during DNA replication rely on the Polalpha/Primase/Ctf4 Complex. *Mol. Cell*, **57**, 812–823.
43. Kim,Y.H., Ishikawa,D., Ha,H.P., Sugiyama,M., Kaneko,Y. and Harashima,S. (2006) Chromosome XII context is important for rDNA function in yeast. *Nucleic Acids Res.*, **34**, 2914–2924.
44. Duffy,E.E., Rutenberg-Schoenberg,M., Stark,C.D., Kitchen,R.R., Gerstein,M.B. and Simon,M.D. (2015) Tracking distinct RNA populations using efficient and reversible covalent chemistry. *Mol. Cell*, **59**, 858–866.
45. Knuppel,R., Kuttenberger,C. and Ferreira-Cerca,S. (2017) Toward time-resolved analysis of RNA metabolism in archaea using 4-thiouracil. *Front. Microbiol.*, **8**, 286.
46. Engel,S.R., Dietrich,F.S., Fisk,D.G., Binkley,G., Balakrishnan,R., Costanzo,M.C., Dwight,S.S., Hitz,B.C., Karra,K., Nash,R.S. *et al.* (2014) The reference genome sequence of Saccharomyces cerevisiae: then and now. *G3 (Bethesda)*, **4**, 389–398.
47. Trapnell,C., Pachter,L. and Salzberg,S.L. (2009) TopHat: discovering splice junctions with RNA-Seq. *Bioinformatics*, **25**, 1105–1111.
48. Anders,S., Pyl,P.T. and Huber,W. (2015) HTSeq–a Python framework to work with high-throughput sequencing data. *Bioinformatics*, **31**, 166–169.
49. Anders,S. and Huber,W. (2010) Differential expression analysis for sequence count data. *Genome Biol.*, **11**, R106.
50. Martin,M. (2011) Cutadapt removes adapter sequences from high-throughput sequencing reads. *EMBnet. J.*, **17**, 10–12.
51. Langmead,B. and Salzberg,S.L. (2012) Fast gapped-read alignment with Bowtie 2. *Nat. Methods*, **9**, 357–359.
52. Zhang,Y., Liu,T., Meyer,C.A., Eeckhoute,J., Johnson,D.S., Bernstein,B.E., Nusbaum,C., Myers,R.M., Brown,M., Li,W. *et al.* (2008) Model-based analysis of ChIP-Seq (MACS). *Genome Biol.*, **9**, R137.
53. Chen,T.W., Li,H.P., Lee,C.C., Gan,R.C., Huang,P.J., Wu,T.H., Lee,C.Y., Chang,Y.F. and Tang,P. (2014) ChIPseek, a web-based analysis tool for ChIP data. *BMC Genomics*, **15**, 539.
54. Shin,H., Liu,T., Manrai,A.K. and Liu,X.S. (2009) CEAS: cis-regulatory element annotation system. *Bioinformatics*, **25**, 2605–2606.
55. Heger,A., Webber,C., Goodson,M., Ponting,C.P. and Lunter,G. (2013) GAT: a simulation framework for testing the association of genomic intervals. *Bioinformatics*, **29**, 2046–2048.
56. Franceschini,A., Szklarczyk,D., Frankild,S., Kuhn,M., Simonovic,M., Roth,A., Lin,J., Minguez,P., Bork,P., von Mering,C. *et al.* (2013) STRING v9.1: protein-protein interaction networks, with increased coverage and integration. *Nucleic Acids Res.*, **41**, D808–D815.
57. Shannon,P., Markiel,A., Ozier,O., Baliga,N.S., Wang,J.T., Ramage,D., Amin,N., Schwikowski,B. and Ideker,T. (2003) Cytoscape: a software environment for integrated models of biomolecular interaction networks. *Genome Res.*, **13**, 2498–2504.

58. Bader,G.D. and Hogue,C.W. (2003) An automated method for finding molecular complexes in large protein interaction networks. *BMC Bioinformatics*, **4**, 2.
59. Huang da,W., Sherman,B.T. and Lempicki,R.A. (2009) Systematic and integrative analysis of large gene lists using DAVID bioinformatics resources. *Nat. Protoc.*, **4**, 44–57.
60. Chatr-Aryamontri,A., Breitkreutz,B.J., Oughtred,R., Boucher,L., Heinicke,S., Chen,D., Stark,C., Breitkreutz,A., Kolas,N., O'Donnell,L. *et al.* (2015) The BioGRID interaction database: 2015 update. *Nucleic Acids Res.*, **43**, D470–D478.
61. Salwinski,L., Miller,C.S., Smith,A.J., Pettit,F.K., Bowie,J.U. and Eisenberg,D. (2004) The Database of Interacting Proteins: 2004 update. *Nucleic Acids Res.*, **32**, D449–D451.
62. Orchard,S., Ammari,M., Aranda,B., Breuza,L., Briganti,L., Broackes-Carter,F., Campbell,N.H., Chavali,G., Chen,C., del-Toro,N. *et al.* (2014) The MIntAct project–IntAct as a common curation platform for 11 molecular interaction databases. *Nucleic Acids Res.*, **42**, D358–D363.
63. Licata,L., Briganti,L., Peluso,D., Perfetto,L., Iannuccelli,M., Galeota,E., Sacco,F., Palma,A., Nardozza,A.P., Santonico,E. *et al.* (2012) MINT, the molecular interaction database: 2012 update. *Nucleic Acids Res.*, **40**, D857–D861.
64. Matys,V., Kel-Margoulis,O.V., Fricke,E., Liebich,I., Land,S., Barre-Dirrie,A., Reuter,I., Chekmenev,D., Krull,M., Hornischer,K. *et al.* (2006) TRANSFAC and its module TRANSCompel: transcriptional gene regulation in eukaryotes. *Nucleic Acids Res.*, **34**, D108–D110.
65. Basha,O., Tirman,S., Eluk,A. and Yeger-Lotem,E. (2013) ResponseNet2.0: Revealing signaling and regulatory pathways connecting your proteins and genes–now with human data. *Nucleic Acids Res.*, **41**, W198–W203.
66. Lan,A., Smoly,I.Y., Rapaport,G., Lindquist,S., Fraenkel,E. and Yeger-Lotem,E. (2011) ResponseNet: revealing signaling and regulatory networks linking genetic and transcriptomic screening data. *Nucleic Acids Res.*, **39**, W424–W429.
67. Yeger-Lotem,E., Riva,L., Su,L.J., Gitler,A.D., Cashikar,A.G., King,O.D., Auluck,P.K., Geddie,M.L., Valastyan,J.S., Karger,D.R. *et al.* (2009) Bridging high-throughput genetic and transcriptional data reveals cellular responses to alpha-synuclein toxicity. *Nat. Genet.*, **41**, 316–323.
68. Angermayr,M., Hochleitner,E., Lottspeich,F. and Bandlow,W. (2007) Protein kinase CK2 activates the atypical Rio1p kinase and promotes its cell-cycle phase-dependent degradation in yeast. *FEBS J.*, **274**, 4654–4667.
69. Angermayr,M. and Bandlow,W. (2002) RIO1, an extraordinary novel protein kinase. *FEBS Lett.*, **524**, 31–36.
70. King,T.H., Decatur,W.A., Bertrand,E., Maxwell,E.S. and Fournier,M.J. (2001) A well-connected and conserved nucleoplasmic helicase is required for production of box C/D and H/ACA snoRNAs and localization of snoRNP proteins. *Mol. Cell. Biol.*, **21**, 7731–7746.
71. Lakshminarasimhan,M., Boanca,G., Banks,C.A., Hattem,G.L., Gabriel,A.E., Groppe,B.D., Smoyer,C., Malanowski,K.E., Peak,A., Florens,L. *et al.* (2016) Proteomic and Genomic Analyses of the Rvb1 and Rvb2 Interaction Network upon Deletion of R2TP Complex Components. *Mol. Cell. Proteomics*, **15**, 960–974.
72. Nano,N. and Houry,W.A. (2013) Chaperone-like activity of the AAA+ proteins Rvb1 and Rvb2 in the assembly of various complexes. *Philos. Trans. R. Soc. Lond. B Biol. Sci.*, **368**, 2011.0399.
73. Kakihara,Y. and Houry,W.A. (2012) The R2TP complex: discovery and functions. *Biochim. Biophys. Acta*, **1823**, 101–107.
74. Forment,J., Mulet,J.M., Vicente,O. and Serrano,R. (2002) The yeast SR protein kinase Sky1p modulates salt tolerance, membrane potential and the Trk1,2 potassium transporter. *Biochim. Biophys. Acta*, **1565**, 36–40.
75. Rodriguez-Lombardero,S., Rodriguez-Belmonte,M.E., Gonzalez-Siso,M.I., Vizoso-Vazquez,A., Valdiglesias,V., Laffon,B. and Cerdan,M.E. (2014) Proteomic analyses reveal that Sky1 modulates apoptosis and mitophagy in Saccharomyces cerevisiae cells exposed to cisplatin. *Int. J. Mol. Sci.*, **15**, 12573–12590.
76. Rodriguez-Lombardero,S., Vizoso-Vazquez,A., Lombardia,L.J., Becerra,M., Gonzalez-Siso,M.I. and Cerdan,M.E. (2014) Sky1 regulates the expression of sulfur metabolism genes in response to cisplatin. *Microbiology*, **160**, 1357–1368.
77. Siebel,C.W., Feng,L., Guthrie,C. and Fu,X.D. (1999) Conservation in budding yeast of a kinase specific for SR splicing factors. *Proc. Natl. Acad. Sci. U.S.A.*, **96**, 5440–5445.
78. Wenz,L.S., Ellenrieder,L., Qiu,J., Bohnert,M., Zufall,N., van der Laan,M., Pfanner,N., Wiedemann,N. and Becker,T. (2015) Sam37 is crucial for formation of the mitochondrial TOM-SAM supercomplex, thereby promoting beta-barrel biogenesis. *J. Cell Biol.*, **210**, 1047–1054.
79. Ponce-Rojas,J.C., Avendano-Monsalve,M.C., Yanez-Falcon,A.R., Jaimes-Miranda,F., Garay,E., Torres-Quiroz,F., DeLuna,A. and Funes,S. (2017) alphabeta'-NAC cooperates with Sam37 to mediate early stages of mitochondrial protein import. *FEBS J.*, **284**, 814–830.
80. Ito,T., Chiba,T., Ozawa,R., Yoshida,M., Hattori,M. and Sakaki,Y. (2001) A comprehensive two-hybrid analysis to explore the yeast protein interactome. *Proc. Natl. Acad. Sci. U.S.A.*, **98**, 4569–4574.
81. Breitkreutz,A., Choi,H., Sharom,J.R., Boucher,L., Neduva,V., Larsen,B., Lin,Z.Y., Breitkreutz,B.J., Stark,C., Liu,G. *et al.* (2010) A global protein kinase and phosphatase interaction network in yeast. *Science*, **328**, 1043–1046.
82. Ptacek,J., Devgan,G., Michaud,G., Zhu,H., Zhu,X., Fasolo,J., Guo,H., Jona,G., Breitkreutz,A., Sopko,R. *et al.* (2005) Global analysis of protein phosphorylation in yeast. *Nature*, **438**, 679–684.
83. Fasolo,J., Sboner,A., Sun,M.G., Yu,H., Chen,R., Sharon,D., Kim,P.M., Gerstein,M. and Snyder,M. (2011) Diverse protein kinase interactions identified by protein microarrays reveal novel connections between cellular processes. *Genes Dev.*, **25**, 767–778.
84. Schafer,T., Strauss,D., Petfalski,E., Tollervey,D. and Hurt,E. (2003) The path from nucleolar 90S to cytoplasmic 40S pre-ribosomes. *EMBO J.*, **22**, 1370–1380.
85. Gilmore,J.M., Sardiu,M.E., Venkatesh,S., Stutzman,B., Peak,A., Seidel,C.W., Workman,J.L., Florens,L. and Washburn,M.P. (2012) Characterization of a highly conserved histone related protein, Ydl156w, and its functional associations using quantitative proteomic analyses. *Mol. Cell. Proteomics*, **11**, M111.011544.
86. Johansson,M.J., He,F., Spatrick,P., Li,C. and Jacobson,A. (2007) Association of yeast Upf1p with direct substrates of the NMD pathway. *Proc. Natl. Acad. Sci. U.S.A.*, **104**, 20872–20877.
87. Lebaron,S., Froment,C., Fromont-Racine,M., Rain,J.C., Monsarrat,B., Caizergues-Ferrer,M. and Henry,Y. (2005) The splicing ATPase prp43p is a component of multiple preribosomal particles. *Mol. Cell. Biol.*, **25**, 9269–9282.
88. Angermayr,M., Roidl,A. and Bandlow,W. (2002) Yeast Rio1p is the founding member of a novel subfamily of protein serine kinases involved in the control of cell cycle progression. *Mol. Microbiol.*, **44**, 309–324.
89. Dosil,M. (2011) Ribosome synthesis-unrelated functions of the preribosomal factor Rrp12 in cell cycle progression and the DNA damage response. *Mol. Cell. Biol.*, **31**, 2422–2438.
90. Kolawa,N., Sweredoski,M.J., Graham,R.L., Oania,R., Hess,S. and Deshaies,R.J. (2013) Perturbations to the ubiquitin conjugate proteome in yeast deltaubx mutants identify Ubx2 as a regulator of membrane lipid composition. *Mol. Cell. Proteomics*, **12**, 2791–2803.
91. Gong,Y., Kakihara,Y., Krogan,N., Greenblatt,J., Emili,A., Zhang,Z. and Houry,W.A. (2009) An atlas of chaperone-protein interactions in Saccharomyces cerevisiae: implications to protein folding pathways in the cell. *Mol. Syst. Biol.*, **5**, 275.
92. Keck,J.M., Jones,M.H., Wong,C.C., Binkley,J., Chen,D., Jaspersen,S.L., Holinger,E.P., Xu,T., Niepel,M., Rout,M.P. *et al.* (2011) A cell cycle phosphoproteome of the yeast centrosome. *Science*, **332**, 1557–1561.
93. Fiedler,D., Braberg,H., Mehta,M., Chechik,G., Cagney,G., Mukherjee,P., Silva,A.C., Shales,M., Collins,S.R., van Wageningen,S. *et al.* (2009) Functional organization of the S. cerevisiae phosphorylation network. *Cell*, **136**, 952–963.
94. Soudet,J., Gelugne,J.P., Belhabich-Baumas,K., Caizergues-Ferrer,M. and Mougin,A. (2010) Immature small ribosomal subunits can engage in translation initiation in Saccharomyces cerevisiae. *EMBO J.*, **29**, 80–92.
95. Sharifpoor,S., van Dyk,D., Costanzo,M., Baryshnikova,A., Friesen,H., Douglas,A.C., Youn,J.Y., VanderSluis,B., Myers,C.L., Papp,B. *et al.* (2012) Functional wiring of the yeast kinome revealed by global analysis of genetic network motifs. *Genome Res.*, **22**, 791–801.

96. Costanzo,M., VanderSluis,B., Koch,E.N., Baryshnikova,A., Pons,C., Tan,G., Wang,W., Usaj,M., Hanchard,J., Lee,S.D. *et al.* (2016) A global genetic interaction network maps a wiring diagram of cellular function. *Science*, **353**, aaf1420.
97. Whitmarsh,A.J. (2007) Regulation of gene transcription by mitogen-activated protein kinase signaling pathways. *Biochim. Biophys. Acta*, **1773**, 1285–1298.
98. Rossetto,D., Avvakumov,N. and Cote,J. (2012) Histone phosphorylation: a chromatin modification involved in diverse nuclear events. *Epigenetics*, **7**, 1098–1108.
99. Banerjee,T. and Chakravarti,D. (2011) A peek into the complex realm of histone phosphorylation. *Mol. Cell. Biol.*, **31**, 4858–4873.
100. Sawicka,A. and Seiser,C. (2014) Sensing core histone phosphorylation - a matter of perfect timing. *Biochim. Biophys. Acta*, **1839**, 711–718.
101. Desai,N., Brown,A., Amunts,A. and Ramakrishnan,V. (2017) The structure of the yeast mitochondrial ribosome. *Science*, **355**, 528–531.
102. Fukasawa,Y., Tsuji,J., Fu,S.C., Tomii,K., Horton,P. and Imai,K. (2015) MitoFates: improved prediction of mitochondrial targeting sequences and their cleavage sites. *Mol. Cell. Proteomics*, **14**, 1113–1126.
103. Quiros,P.M., Mottis,A. and Auwerx,J. (2016) Mitonuclear communication in homeostasis and stress. *Nat. Rev. Mol. Cell Biol.*, **17**, 213–226.
104. Bohovych,I. and Khalimonchuk,O. (2016) Sending out an SOS: mitochondria as a signaling hub. *Front. Cell Dev. Biol.*, **4**, 109.
105. Li,S.C. and Kane,P.M. (2009) The yeast lysosome-like vacuole: endpoint and crossroads. *Biochim. Biophys. Acta*, **1793**, 650–663.
106. Armstrong,J. (2010) Yeast vacuoles: more than a model lysosome. *Trends Cell Biol.*, **20**, 580–585.
107. Okada,N., Ogawa,J. and Shima,J. (2014) Comprehensive analysis of genes involved in the oxidative stress tolerance using yeast heterozygous deletion collection. *FEMS Yeast Res.*, **14**, 425–434.
108. Hahn,J.S., Hu,Z.Z., Thiele,D.J. and Iyer,V.R. (2004) Genome-wide analysis of the biology of stress responses through heat shock transcription factor. *Mol. Cell. Biol.*, **24**, 5249–5256.
109. Romero-Santacreu,L., Moreno,J., Perez-Ortin,J.E. and Alepuz,P. (2009) Specific and global regulation of mRNA stability during osmotic stress in Saccharomyces cerevisiae. *RNA*, **15**, 1110–1120.
110. Conway,M.K., Grunwald,D. and Heideman,W. (2012) Glucose, nitrogen, and phosphate repletion in Saccharomyces cerevisiae: common transcriptional responses to different nutrient signals. *G3*, **2**, 1003–1017.
111. Tkach,J.M., Yimit,A., Lee,A.Y., Riffle,M., Costanzo,M., Jaschob,D., Hendry,J.A., Ou,J., Moffat,J., Boone,C. *et al.* (2012) Dissecting DNA damage response pathways by analysing protein localization and abundance changes during DNA replication stress. *Nat. Cell Biol.*, **14**, 966–976.
112. Hinnebusch,A.G. (2005) Translational regulation of GCN4 and the general amino acid control of yeast. *Annu. Rev. Microbiol.*, **59**, 407–450.
113. Hinnebusch,A.G. (1985) A hierarchy of trans-acting factors modulates translation of an activator of amino acid biosynthetic genes in Saccharomyces cerevisiae. *Mol. Cell. Biol.*, **5**, 2349–2360.
114. Shemer,R., Meimoun,A., Holtzman,T. and Kornitzer,D. (2002) Regulation of the transcription factor Gcn4 by Pho85 cyclin PCL5. *Mol. Cell. Biol.*, **22**, 5395–5404.
115. Kornitzer,D., Raboy,B., Kulka,R.G. and Fink,G.R. (1994) Regulated degradation of the transcription factor Gcn4. *EMBO J.*, **13**, 6021–6030.
116. Natarajan,K., Meyer,M.R., Jackson,B.M., Slade,D., Roberts,C., Hinnebusch,A.G. and Marton,M.J. (2001) Transcriptional profiling shows that Gcn4p is a master regulator of gene expression during amino acid starvation in yeast. *Mol. Cell. Biol.*, **21**, 4347–4368.
117. Lempiainen,H. and Shore,D. (2009) Growth control and ribosome biogenesis. *Curr. Opin. Cell Biol.*, **21**, 855–863.
118. Powers,T. and Walter,P. (1999) Regulation of ribosome biogenesis by the rapamycin-sensitive TOR-signaling pathway in Saccharomyces cerevisiae. *Mol. Biol. Cell*, **10**, 987–1000.
119. Smedley,D., Haider,S., Durinck,S., Pandini,L., Provero,P., Allen,J., Arnaiz,O., Awedh,M.H., Baldock,R., Barbiera,G. *et al.* (2015) The BioMart community portal: an innovative alternative to large, centralized data repositories. *Nucleic Acids Res.*, **43**, W589–W598.
120. Hinnebusch,A.G. and Fink,G.R. (1983) Positive regulation in the general amino acid control of Saccharomyces cerevisiae. *Proc. Natl. Acad. Sci. U.S.A.*, **80**, 5374–5378.
121. Xie,Y. and Varshavsky,A. (2001) RPN4 is a ligand, substrate, and transcriptional regulator of the 26S proteasome: a negative feedback circuit. *Proc. Natl. Acad. Sci. U.S.A.*, **98**, 3056–3061.
122. Barandun,J., Chaker-Margot,M., Hunziker,M., Molloy,K.R., Chait,B.T. and Klinge,S. (2017) The complete structure of the small-subunit processome. *Nat. Struct. Mol. Biol.*, **24**, 944–953.
123. Chaker-Margot,M., Barandun,J., Hunziker,M. and Klinge,S. (2017) Architecture of the yeast small subunit processome. *Science*, **355**, eaal1880.
124. Tsuboi,T., Kuroha,K., Kudo,K., Makino,S., Inoue,E., Kashima,I. and Inada,T. (2012) Dom34:hbs1 plays a general role in quality-control systems by dissociation of a stalled ribosome at the 3′ end of aberrant mRNA. *Mol. Cell*, **46**, 518–529.
125. Kobayashi,T., Heck,D.J., Nomura,M. and Horiuchi,T. (1998) Expansion and contraction of ribosomal DNA repeats in Saccharomyces cerevisiae: requirement of replication fork blocking (Fob1) protein and the role of RNA polymerase I. *Genes Dev.*, **12**, 3821–3830.
126. Kobayashi,T. and Ganley,A.R. (2005) Recombination regulation by transcription-induced cohesin dissociation in rDNA repeats. *Science*, **309**, 1581–1584.
127. Romano,G.H., Harari,Y., Yehuda,T., Podhorzer,A., Rubinstein,L., Shamir,R., Gottlieb,A., Silberberg,Y., Pe'er,D., Ruppin,E. *et al.* (2013) Environmental stresses disrupt telomere length homeostasis. *PLos Genet.*, **9**, e1003721.
128. Yamada,M., Hayatsu,N., Matsuura,A. and Ishikawa,F. (1998) Y'-Help1, a DNA helicase encoded by the yeast subtelomeric Y' element, is induced in survivors defective for telomerase. *J. Biol. Chem.*, **273**, 33360–33366.
129. Albuquerque,C.P., Smolka,M.B., Payne,S.H., Bafna,V., Eng,J. and Zhou,H. (2008) A multidimensional chromatography technology for in-depth phosphoproteome analysis. *Mol. Cell. Proteomics*, **7**, 1389–1396.
130. Ljungdahl,P.O. and Daignan-Fornier,B. (2012) Regulation of amino acid, nucleotide, and phosphate metabolism in Saccharomyces cerevisiae. *Genetics*, **190**, 885–929.
131. Harbison,C.T., Gordon,D.B., Lee,T.I., Rinaldi,N.J., Macisaac,K.D., Danford,T.W., Hannett,N.M., Tagne,J.B., Reynolds,D.B., Yoo,J. *et al.* (2004) Transcriptional regulatory code of a eukaryotic genome. *Nature*, **431**, 99–104.
132. Ostrow,A.Z., Nellimoottil,T., Knott,S.R., Fox,C.A., Tavare,S. and Aparicio,O.M. (2014) Fkh1 and Fkh2 bind multiple chromosomal elements in the S. cerevisiae genome with distinct specificities and cell cycle dynamics. *PLoS One*, **9**, e87647.
133. Hill,D.E., Hope,I.A., Macke,J.P. and Struhl,K. (1986) Saturation mutagenesis of the yeast his3 regulatory site: requirements for transcriptional induction and for binding by GCN4 activator protein. *Science*, **234**, 451–457.
134. Arndt,K. and Fink,G.R. (1986) GCN4 protein, a positive transcription factor in yeast, binds general control promoters at all 5′ TGACTC 3′ sequences. *Proc. Natl. Acad. Sci. U.S.A.*, **83**, 8516–8520.
135. Oliphant,A.R., Brandl,C.J. and Struhl,K. (1989) Defining the sequence specificity of DNA-binding proteins by selecting binding sites from random-sequence oligonucleotides: analysis of yeast GCN4 protein. *Mol. Cell. Biol.*, **9**, 2944–2949.
136. Kulak,N.A., Pichler,G., Paron,I., Nagaraj,N. and Mann,M. (2014) Minimal, encapsulated proteomic-sample processing applied to copy-number estimation in eukaryotic cells. *Nat. Methods*, **11**, 319–324.
137. Ghaemmaghami,S., Huh,W.K., Bower,K., Howson,R.W., Belle,A., Dephoure,N., O'Shea,E.K. and Weissman,J.S. (2003) Global analysis of protein expression in yeast. *Nature*, **425**, 737–741.
138. Efeyan,A., Comb,W.C. and Sabatini,D.M. (2015) Nutrient-sensing mechanisms and pathways. *Nature*, **517**, 302–310.
139. Sancak,Y., Bar-Peled,L., Zoncu,R., Markhard,A.L., Nada,S. and Sabatini,D.M. (2010) Ragulator-Rag complex targets mTORC1 to the lysosomal surface and is necessary for its activation by amino acids. *Cell*, **141**, 290–303.

140. Hardie,D.G., Ross,F.A. and Hawley,S.A. (2012) AMPK: a nutrient and energy sensor that maintains energy homeostasis. *Nat. Rev. Mol. Cell Biol.*, **13**, 251–262.
141. Weems,A.D., Johnson,C.R., Argueso,J.L. and McMurray,M.A. (2014) Higher-order septin assembly is driven by GTP-promoted conformational changes: evidence from unbiased mutational analysis in Saccharomyces cerevisiae. *Genetics*, **196**, 711–727.
142. King,K., Jin,M. and Lew,D. (2012) Roles of Hsl1p and Hsl7p in Swe1p degradation: beyond septin tethering. *Eukaryot. Cell*, **11**, 1496–1502.
143. Suzuki,C., Takahashi,K., Hayama,S., Ishikawa,N., Kato,T., Ito,T., Tsuchiya,E., Nakamura,Y. and Daigo,Y. (2007) Identification of Myc-associated protein with JmjC domain as a novel therapeutic target oncogene for lung cancer. *Mol. Cancer Ther.*, **6**, 542–551.
144. Tansey,W.P. (2014) Mammalian MYC proteins and cancer. *New J. Sci.*, **2014**, 757534.
145. Forbes,S.A., Beare,D., Gunasekaran,P., Leung,K., Bindal,N., Boutselakis,H., Ding,M., Bamford,S., Cole,C., Ward,S. *et al.* (2015) COSMIC: exploring the world's knowledge of somatic mutations in human cancer. *Nucleic Acids Res.*, **43**, D805–D811.
146. Dang,C.V. (2013) MYC, metabolism, cell growth, and tumorigenesis. *Cold Spring Harb. Perspect. Med.*, **3**, a014217.